Desalination 533 (2022) 115782

Contents lists available at ScienceDirect

Desalination

journal homepage: www.elsevier.com/locate/desal

Boron carbon nitride nanosheets in water and wastewater treatment: A critical review

Yasar K. Recepoglu [a], A. Yagmur Goren [b], Vahid Vatanpour [c,d], Yeojoon Yoon [e,*], Alireza Khataee [f,g,**]

[a] Department of Chemical Engineering, Izmir Institute of Technology, 35430 Urla, Izmir, Turkey
[b] Department of Environmental Engineering, Izmir Institute of Technology, 35430 Urla, Izmir, Turkey
[c] Department of Applied Chemistry, Faculty of Chemistry, Kharazmi University, 15719-14911 Tehran, Iran
[d] Environmental Engineering Department, Istanbul Technical University, Maslak, 34469 Istanbul, Turkey
[e] Department of Environmental and Energy Engineering, Yonsei University, 1, Yonseidae-gil, Wonju-si 26493, Gangwon-do, Republic of Korea
[f] Department of Environmental Engineering, Gebze Technical University, 41400 Gebze, Turkey
[g] Research Laboratory of Advanced Water and Wastewater Treatment Processes, Department of Applied Chemistry, Faculty of Chemistry, University of Tabriz, 51666-16471 Tabriz, Iran

HIGHLIGHTS

- BCN nanosheets improved performance for water treatment is summarized.
- Synthesis methods for ternary BCN nanosheets are explored.
- BCN as photocatalysts, adsorbents, and in electrochemical reduction are discussed.
- Metal-loaded BCN nanosheets were elaborated as effective water treatment strategy.
- Metal and ammonia production potential of BCN increased with metal modification.

GRAPHICAL ABSTRACT

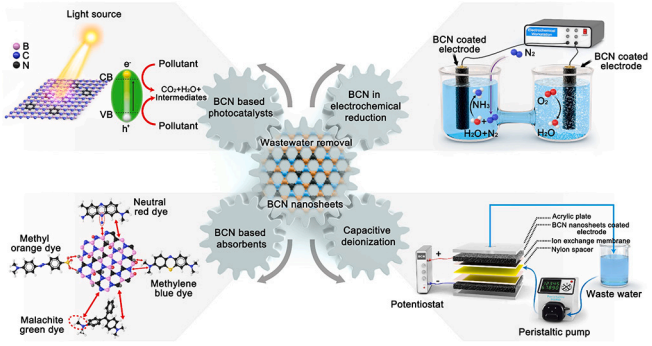

ARTICLE INFO

ABSTRACT

Abbreviations: AG, acid green AG; ADS, adsorptive desulfurization; IBAD, ion beam assisted deposition; B, boron; BCN, boron carbon nitride; BN, boron nitride; BN-CN, boron nitride-carbon nitride; CDI, capacitive deionization; C, carbon; CVD, chemical vapor deposition; CR, Congo red; BCN (BCN@Cu), copper (Cu) nanoparticles embedded in BCN; Cu-BCN, copper loaded BCN; CV, crystal violet; BCN@Cu/CNT, Cu with BCN on carbon nanotube; DW, distilled water; FE, Faraday efficiency; FT/BCN, Fe@TiO_2/BCN; F, Freundlich isotherm; GCN, graphitic-carbon nitride; h-BN, hexagonal shape; L, Langmuir isotherm; LCVD, laser CVD; LBE, liquid-based direct exfoliation; LPCVD, low-pressure CVD; MG, malachite green; MO, methyl orange; NR, neutral red; BCN@Ni-Ni, Ni nanoparticle and single atom Ni on BCN; BCN@Ni, Ni-doped BCN catalyst; N, nitrogen; PECVD, plasma-enhanced CVD; PTFE, poly(tetrafluoroethylene); PFO, pseudo-first order; PSO, pseudo second-order; PLD, pulsed laser deposition; BCN-PA, pyromellitic dianhydride; RF, radio frequency; RNB, reactive navy blue; RO, reverse osmosis; RhB, rhodamine B; RW, river water; SBCN, solvothermal route; SS, synthetic solution; TC, tetracycline; TBCN, thermal condensation; TOC, total organic carbon; 2D, two dimensional.

* Corresponding author.
** Correspondence to: A. Khataee, Department of Environmental Engineering, Gebze Technical University, 41400 Gebze, Turkey.
E-mail addresses: yajoony@yonsei.ac.kr (Y. Yoon), a_khataee@tabrizu.ac.ir (A. Khataee).

https://doi.org/10.1016/j.desal.2022.115782
Received 6 March 2022; Received in revised form 8 April 2022; Accepted 10 April 2022
Available online 19 April 2022

Keywords:
Adsorption
Ammonia production
Boron carbon nitride
Electrochemical reduction
Photocatalyst

The availability and accessibility of clean and secure water supplies are pressing technological and scientific issues worldwide. As a result of global water constraints, wastewater treatment and reuse are being evaluated as feasible alternatives to fresh water for agricultural irrigation and domestic and industrial purposes. Boron carbon nitride (BCN) nanosheets have been studied intensively in the last decade in batteries, biosensors, and capacitors, and for use as catalysts, and they have recently been used in wastewater treatment. BCN materials, along with their synthesis processes, characteristics, and application areas in water and wastewater treatment, are discussed thoroughly in this paper. Additionally, synthesis processes for ternary BCN compounds, including chemical vapor deposition, ion beam-aided deposition, magnetron sputtering, and pulsed laser deposition, are described. BCN materials have also been explored because of their flexible electrical features, excellent mechanical strength, outstanding unreactivity, and significant stability, which make them appropriate for a range of severe environment applications. Thus, the use of BCN materials as photocatalysts and adsorbents and in electrochemical reduction and capacitive deionization are also discussed thoroughly. The highest ammonia production of 172,226.5 μg/h.mg.cat and faradic efficiency of 95.3% have been obtained using the BCN@Cu/CNT catalyst, whereas the ammonia production and FE values for metal-free BCN are 7.75 μg/h.mg.cat and 13.8%. Moreover, the maximum attained adsorption capacities of BCN nanosheets for Pb^{2+} and Hg^{2+} are 210 and 625 mg/g, respectively. Overall, this review indicates that essential work on BCN nanosheets is still needed. Future research should focus on the development of BCN nanostructures to encourage multidisciplinary research.

1. Introduction

In recent years, water pollution has emerged as a global issue, posing a severe threat to ecosystems and the environment. In particular, wastewaters containing hazardous heavy metals, oils, solvents, and dyes with aromatic rings have exacerbated water problems and caused health risks due to population growth and rapid industrial development [1,2]. Water decontamination has been performed in various ways, including flocculation, adsorption, chemical oxidation, and photocatalysis [3–6]. On the other hand, most of these treatment methods have several disadvantages, including high chemical consumption and sludge production, high maintenances and operational cost, high energy consumption, the requirement of additional pre-treatment systems, and requirement of pH adjustment. However, it has proven difficult to develop nanomaterials with flexible properties that are desirable for meeting the growing demand for solutions to environmental problems worldwide. Only clean and cost-effective energy generation/storage technologies will allow us to achieve this goal [7–10].

To date, carbonaceous materials such as fullerenes, nanotubes, graphene, and nanodiamond have contributed to the advancement of science through the construction of units with extraordinary features, including high surface areas and porous structures, and have drawn ongoing attention for energy and waste treatment applications [11,12]. Among these, low-cost and efficient metal-free nanomaterials, which consist mostly of carbon (C), nitrogen (N), or boron (B), have been commonly used for the adsorption of harmful contaminants [13]. Boron nitride (BN) nanosheets, graphene-like nanomaterials with alternating B and N atoms, have excellent adsorption properties for several of the aforementioned contaminants. The hexagonal BN (h-BN) possesses an analogous layered structure with in-plane covalent bonds (σ-bonds) and out-of-plane van der Waals interactions. However, due to the electronegativity difference between B and N, the σ bonds are partially ionic and interlayer forces are “lip-lip” interactions [14]. The BN films have piqued the interest of researchers because to their extremely desired mechanical, thermal, electrical, and optical characteristics. Depending on the preparation circumstances, the structure of the films can be cubic (c-BN), wurtzite (w-BN), h-BN, turbostratic (t-BN), or amorphous (a-BN), among others. Because of the crystalline structural similarities between graphite and h-BN, as well as diamond and c-BN, the synthesis of boron carbon nitride (BCN) compounds with diverse compositions has been undertaken successfully in recent years. Previous studies have demonstrated that the tension in BCN films is often substantially lower than that in c-BN films which will lead to improved film adhesion. The unique atomic configurations of ternary BCN compounds tend to generate a more stable and less strained structure [15]. Unlike h-BN which has a large bandgap of 5 eV, the computed direct bandgap of BCN monolayer is 1.18 eV, which is beneficial for use in optoelectronic applications [16]. The hexagonal and cubic polymorphs of BN are the same. In comparison to C and BN, hybrid compounds made of three elements, B, C, and N, are appealing due to the anticipation of intermediate or even better qualities. Cubic BCN compounds would be made by transforming hexagonal BCN compounds under high-pressure and high-temperature (HP/HT) conditions, similar to how diamond and cBN are made from their hexagonal polymorphs [17]. Moreover, graphitic-carbon nitride (CN) has been investigated extensively for potential applications in energy and biosensors. However, CN nanomaterials for cleaning water have received less interest due to poor interfacial features, including water insolubility, low active surface area, and limited functional groups [18–22]. Thus, a novel material combining the benefits of graphene, BN nanosheets, and CN analogs was developed. With their polymorphic structures, BCN ternary compounds exhibit a broad range of physical properties because the layered structure resembles graphite [23].

BCN can be employed as an intercalation material in Li-ion batteries [24,25]. BCN is distinguished not only by the fact that its composition can be tuned using various synthesizing processes but also because each BCN composition has its own set of properties. This has drawn widespread attention in both academia and industry, paving the way for BCN uses in electrical (transistor, capacitor, photodetector) [26–28], optical (UV detector) [29], and mechanical (low friction coefficient, excellent wear resistance, and high hardness, making it useful for protective antiwear coating) applications [30,31]. BCN nanomaterials have been used effectively for water treatment because of their excellent adsorption abilities. Organic dyes are significant water pollutants generated by the food, paper, leather, and textile industries, and dye wastewater has complex components, high organic contents and COD concentrations, and a large number of refractory compounds that must be removed before discharge [32,33]. Mesoporous BCN has been used to treat malachite green (MG) from water and showed a maximum adsorption capacity of 310 mg/g [34]. Additionally, porous BCN nanosheets have shown exceptional photodegradation capacities for organic pollutant decontamination. BCN materials have also been used in the nuclear power industry to enrich uranium residues by reducing the uranyl ions, which are highly soluble and mobile ($U(VI)O_2^{2+}$), to sparingly soluble U (IV) as oxides/hydroxides with photocatalytic activities [35].

In this review, for the first time to the best of our knowledge, BCN materials are elucidated in detail, considering their synthesis methods, properties, and application areas in water and wastewater treatment. The related BCN papers reviewed in this perspective were collected from Scopus database with keywords of “boron carbon nitride” searched in “TITLE-ABS-KEY” for all years. Next, all found papers were checked for selecting papers related to water and wastewater treatment. Most of the published papers in this field are related to the last five years. To facilitate development of ternary BCN compounds, synthesis procedures

such as ion beam assisted deposition (IBAD), chemical vapor deposition (CVD), pulsed laser deposition (PLD), and magnetron sputtering are explained in detail. BCN materials are also discussed in the contexts of their flexible electrical characteristics, excellent mechanical strength, exceptional unreactivity, and high thermal durability, which make them ideal for various harsh environment applications. This article also sheds light on applications of BCN materials as photocatalysts, adsorbents, in electrochemical reduction, and in other processes such as capacitive deionization. Future perspectives are also presented as crucial advice for developing BCN nanostructures to spark future research for interdisciplinary applications.

2. Boron carbon nitride

2.1. Definition and properties

BCN is a new semiconductor material with the high thermal and chemical stabilities of h-BN [36]. The ternary BCN semiconductor has conjugated sp^2 hybridized C atoms connected in a honeycomb lattice (i.e., an electron system) with C inserted into the lattice. Understanding the compositional triangle of the BCN system is required for synthesizing well-controlled three-phase BCN ternary systems and reducing thermodynamically unstable segregations [14]. The corners of the triangles correspond to the pure phases, when pure graphitic structures in general, and graphene in particular, are regarded at C. The B corner would be occupied by freshly created synthetic borophene. However, it is thermodynamically unstable, very poisonous, and in the early phases of development. Moving from C to B produces a variety of metastable intermediary phases, the most stable of which are B_4C, BC_2 and BC_3. These phases are primarily created by introducing B atoms into the diamond structure at various lattice locations and in diverse amounts. B_4C, for example, has a diamond lattice structure, but BC_3 primitive cells can be tetragonal or trigonal depending on the synthesis temperature and pressure. It should be noted that the BC regions are sp^3 hybridized, which may disrupt the two-dimensional (2D) arrangement desired for BCN films. The C_3N_4 may be seen along the CN side of the triangle. CN has a layered structure and is made up of strong covalent connections between N and C atoms. The initial set of N-atoms (N_1) in each layer have a sp^2 configuration and are bound to 3-coordinated C atoms. Then, in a 1,3,5 triazine ring, C atoms are sp^2 hybridized with 2-coordinated N atoms (N_2) to produce a layer of graphitic-C_3N_4. As a result, assuming the creation of CN zones in the final structure, the film's two-dimensionality will be retained. The bottom side of the triangle shows BN nanosized morphologies, while the center point denotes a 1:1 B:N stoichiometry ratio. If the thickness and atomic ratios of B, C, and N are well-controlled at the BCN center point, 2D h-BCN may be produced. However, rigorous monitoring of atomic ratios in all circumstances is difficult, therefore the final composition may depart from B:C:N 1:1:1. The bandgap of BCN (>5.0 eV) can be finely regulated to maximize its catalytic functions by altering the degree of C integration. BCN semiconductors have been shown to be active photocatalysts for visible-light target photoredox processes such as H_2O splitting and CO_2 reduction [35,37,38]. Layered h-BN is structurally similar to graphene, a well-known 2D substance, and has unique absorption, mechanical, optical thermoelectric, and electrical properties, such as strong charge carrier mobility and a room-temperature quantum Hall effect, giving it tremendous potential in the nanoelectronics sector [39]. Ternary BCNs are hybrid forms of h-BN and graphene that have the potential to create bandgaps, which are essential in numerous applications, such as luminescence, electronics, and solar energy converters [40]. BCN has also been used as a carbon-based catalyst in aerobic oxidative dehydrogenation reactions (ODH) such as ethylbenzene dehydrogenation because carbon insertion considerably increases the surface area of h-BN [41]. Moreover, BCN derived from isostructural h-BN has been employed in ferromagnetism, hydrogen storage, and impurity adsorption and has also been applied as an electrocatalyst for nitrogen reduction reactions to decrease the high energy consumption and CO_2 emission [42].

2.2. Synthesis methods

It's proven difficult to develop nanomaterials with desirable tunable qualities to meet the growing demand for solutions to environmental problems throughout the world. Only clean and cost-effective energy generation/storage technologies will allow us to reach this aim. A number of methods for synthesizing BCN structures of varied dimensionalities have been documented over time. The molten hydroxide, liquid-based direct exfoliation (LBE), CVD, magnetron sputtering, PLD, and IBAD methods have been used to fabricate BCNs [30,39]. This section focuses on the synthesis techniques including important process parameters and their effects on elemental composition and properties of BCN.

2.2.1. Molten hydroxide method

The molten hydroxide method is a simple process in which commonly used molten salts can be utilized to exfoliate h-BN bulk materials in a top-down method to exfoliate h-BN layer-by-layer and chemically obtain BCN. The exfoliation process includes the self-curling of the sheets, insertion of hydroxides, cutting by the reaction of h-BN and hydroxides, and natural peeling away from the parent materials. In this method, the high chemical potentials of the cations (Na^+ or K^+) and anions (OH^-) are linked to their insertion into the interlayer gap on the top surface. Furthermore, the self-curling of the BN nanosheets aids the insertion of cations and anions. Cations adsorb preferentially onto a negatively curved surface, whereas anions adsorb preferentially onto a positively curved surface. In a typical procedure, NaOH:KOH (molar ratio = 51.5:48.5) is thoroughly mixed, followed by the addition of h-BN powder, which is then ground to a homogenous form. The mixture is then transferred to a stainless steel autoclave lined with poly(tetrafluoroethylene) (PTFE) and heated at 180 °C for 2 h. This approach has several advantages, including abundance of raw materials, cost-effectiveness, ease of operation, and high yields [43].

2.2.2. Liquid based direct exfoliation (LBE)

Under moderate conditions, LBE is a suitable approach for creating high-quality 2D nanomaterials. LBE refers to a series of procedures for exfoliating bulk-layered materials into thin flakes of 2D nanomaterials in liquid media with little or no chemical reaction while maintaining high crystallinity. This includes liquid-phase exfoliation using ionic liquids, surfactants, and salts, electrochemical exfoliation in different liquid media, and extensive reliance on liquid media for exfoliation. LBE is a flexible approach for producing inexpensive nanosheets. Layered powder can be converted into large numbers of nanosheets using various techniques (including intercalation, sonication/shear, and centrifugation). Shear exfoliation may yield industrial-scale volumes and speeds of nanosheet fabrication, making the technique scalable. Because the input energy is almost exclusively employed to exfoliate and cut the nanosheets (i.e., form edges) rather than create point defects, the final nanosheets are almost entirely free of defects. Solvents, ionic liquids, surfactants, and polymers have been used to exfoliate h-BN effectively using LBE. As a result, nanosheets can be formed in aqueous media or different organic solvents. The vast range of solvent solutions that arise helps with nanosheet dispersion. Nanosheet dispersions can be formed into networks or filaments using several techniques, including inkjet printing [44].

2.2.3. Chemical vapor deposition (CVD)

CVD is one of the most prevalent methods for depositing BCNs. CVD has long been recognized as an attractive deposition method because of the high-quality film it generates and the relative ease with which it can control both the microstructure and composition of the materials. The volatile precursors react to deposit the necessary coating on the surface of the substrate during CVD. During the CVD process, extremely volatile

by-products are often generated and eliminated by flowing gas through the chamber where the reaction occurs. The CVD process has undergone various changes over the years, including laser CVD (LCVD) [45], plasma-enhanced CVD (PECVD) [46], low-pressure CVD (LPCVD) [47], and microwave plasma-assisted CVD (MPCVD) [48]. In addition, CVD can be separated into three classes depending on the precursor used: boron trichloride-based CVD [49], diborane-based CVD [50], and organoboron compound-based CVD [30]. Namely, Yuki et al. [51] prepared BCN films synthesized by plasma-assisted chemical vapor deposition (PACVD). In this context, Using a PACVD device with a horizontal quartz reactor, the BCN film was produced on fused silica and p-type Si (8–12 Ω.cm) substrates. As source gases, BCl_3, N_2, and CH_4 were employed. The substrate was put on a holder after it had been reduced and chemically treated. An external furnace heated the substrate to 650 °C, and it was negatively DC-biased at 200 V. Inductive coupling was used to initiate the plasma 15 cm away from the substrate in an N_2 and CH_4 combination at 13.56 MHz. Before BCN deposition, the substrate surface was cleaned with H_2 plasma for 3 min. The radio-frequency (RF) power was set to 40 watts. Separate from the N_2 and CH_4 provided to sustain the plasma, a combination of BCl_3 and H_2 gases was added near the substrate. The atomic N/B flow rate ratio was set to 2.5, and the BCl_3 mass flow rate was set to 0.8 sccm. 1.0 Torr was selected as the total gas pressure. For a 2 h growth time, BCN films with thicknesses ranging from 100 to 300 nm were produced.

2.2.4. Magnetron sputtering

The most common technique for fabricating boron-containing coatings with a planar magnetron is to use a boron-containing compound target. A non-boron component is utilized to acquire the required boron compound layer directly and thus use the electrical conductivity of the target. When operated in a nitrogen atmosphere, pure boron magnetron targets have been primarily used in semiconductor doping technology to deposit boron nitride films via reactive magnetron sputtering. On the other hand, pure boron exhibits low electrical conductivity. As with any other dielectric target, this causes many problems, such as target surface charge-up and enhanced arcing. Sputtering magnetrons with dielectric targets typically operate at the conventional radio frequency (RF) of 13.56 MHz [52]. For example, BCN films were deposited on silicon wafers by RF magnetron sputtering of boron and graphite targets. For this, high-quality graphite (99.99%) and B (99.9%) targets with diameters of 2 in. were employed as C and B sources, respectively, while Si (1 0 0) wafers were chosen as the substrate material. During deposition, the gap between the targets and the substrate was kept constant at 50 mm. The deposition chamber had a base pressure of less than 1×10^{-3} Pa and a working pressure of around 1 Pa, with a sputtering gas combination of N_2 and Ar (50:50). The thickness of the BCN films formed on the substrate ranged between 300 and 500 nm. For BCN film deposition, the boron target's sputtering power was adjusted to 150 W, while the carbon target's sputtering power was varied from 60 to 240 W. Substrate bias was not used, and the substrate was not intentionally heated during the deposition. The Si substrates were cleaned ultrasonically in acetone and methanol before being blow-dried with nitrogen gas. Prior to deposition, the substrate was in situ sputtered in argon plasma for 5 min with a 150 W RF bias [53].

2.2.5. Pulsed laser deposition (PLD)

In PLD, a high-power laser beam is periodically focused onto a target material, producing instantaneous evaporation and ionization of the surface atoms and, as a result, forming a concentrated plasma inside the plume of the evaporated material. These atoms, electrons, and ions are propelled away from their target and collide with the surface of the substrate, forming thin coatings with the same chemical composition as the evaporated substance. In addition, gas molecules can be supplied into the reaction chamber to react with the atoms or molecules in the plume and thus deposit a coating with the appropriate chemical composition on the substrate surface. Even when inert gases are used, increasing the deposition pressure limits plume growth by increasing the number of molecules colliding with the plume, allowing for uniform deposition across many square centimeters of the substrate surface [54]. As an example of this method, Ling et al. [55] prepared BCN thin films on Si (1 0 0) substrates by means of plasma-assisted pulsed laser deposition at low temperatures (<80 °C). At 10 Hz, laser pulses of the second harmonic of a Q-switched Nd/YAG laser ($\lambda = 532$ nm, $\tau_{FWHM} = 15$ ns) were utilized to ablate the target at 45 °C to the target normal. To avoid the production of deep craters on the target surface, the target was kept revolving at multiple rpm. As substrates, polished Si (1 0 0) wafers with a resistivity of 5 Ω.cm were employed. To remove surface impurities and the oxide layer, the Si substrates were supersonically cleaned in acetone and immersed in a 10% HF solution. The target and the substrate were separated by 4 cm. Target ablation and film preparation were carried out downstream of the N_2 plasma created by an ECR microwave discharge in pure (>99.9%) N_2 gas at a working pressure of 3×10^{-2} Pa. On the target surface, the laser fluence was approximately 5 J/cm^2. The substrates were kept at room temperature, which normally reached no more than 80 °C due to the bombardment by the plasma stream during film formation.

2.2.6. Ion beam assisted deposition (IBAD)

IBAD entails simultaneous thin film deposition and directed ion bombardment. Evaporation, laser deposition, or ion beam sputtering are standard methods for delivering neutral species through PVD. The thermal energy of evaporated neutrals is generally 0.1–0.2 eV, but the energy of sputtered neutrals can be several electron volts. Directed ions interact with impinging neutrals via physicochemical contact at the substrate surface, generating energy transfer between the particles. The significant impact of nonreactive IBAD with inert gases, such as Ar, is to enhance the energy of neutral atoms by collisions with energetic inert ions. Reactive IBAD produces nitrides or oxides of evaporated metal by utilizing reactive gases such as nitrogen or oxygen [56]. For instance, BCN coatings were deposited on Si (1 0 0) wafers and Si_3N_4 disks by using ion beam assisted deposition from a boron carbide target. To do this, a 99.99% pure B_4C target was placed in the electron beam evaporator, and a substrate jig with Si wafer (Si_3N_4 disk) was positioned on the substrate holder. Following that, the vacuum chamber was evacuated to less than 2×10^{-4} Pa. For further cleaning, the sample surface was blasted with nitrogen ions for 5 min. At 1 kV (A.V.) and 100 μA/cm^2, nitrogen ions were produced (A.C.D.). The BCN coatings were then created by combining B gas, C vapor, and energetic N ions. At 1–2 kV (A.V.) and 30–90 μA/cm^2, powerful N ions were generated (A.C.D.). The B and C vapors were created by using an electron beam evaporator to heat a B_4C target. BCN coating deposition rates were 0.5 and 1.0 nm/s, which were adjusted by altering the vapor emission current. All of the BCN coatings were roughly 300 nm thick [57].

Among the above-mentioned synthesis methods, PLD and IBAP methods are not very promising because they need gases such as nitrogen, nitrogen, and oxygen, which cause increased costs during synthesis and can cause difficulties in operation, although the material is produced efficiently. Similarly, the LBE method is unsuitable for commercial applications due to the high cost and possible toxic effects of chemicals such as polymers, surfactants, and solvents used during synthesis. The most significant drawback of the magnetron sputtering method is the high energy cost due to the electrical potential applied during synthesis. On the other hand, the low/medium temperature synthesis techniques, particularly CVD techniques, are inexpensive, offer great flexibility, and are the easiest to scale up to commercial production. Moreover, CVD procedures are dependable in retaining the repeatability of the final chemical composition due to procedural control over precursor concentrations, temperature, flow rates, and substrates.

3. Application of boron carbon nitride in water and wastewater treatment

The utilization of BCN nanosheets in wastewater treatment, along with their production methods, removal performances, adsorption capacities, readabilities, and potential for value-added material generation, is discussed in great detail in the following sections. The flexible electrical characteristics, superior mechanical stability, superior chemical resistance, and excellent thermal conductivity of BCN materials, making them suitable for various severe environmental applications, have also been investigated. Moreover, the advantages and disadvantages of integrating BCN nanosheets with conventional water and wastewater treatment processes have been discussed.

3.1. BCN based photocatalysts

Waste discharge has increased as a result of global industrialization and urbanization. Environmental pollution on a worldwide scale, such as greenhouse gas and NOx emissions and water contamination, is approaching alarming levels. Graphitic carbon nitride-based materials have gained interest as visible-light-responsive photocatalysts for organic pollutants, microbial degradation, CO_2 reduction, and NO_x abatement [58–61]. Furthermore, increasing global energy use contributes to climate change and the energy crisis, which are serious concerns. Hydrogen synthesis by photocatalytic splitting of water is a feasible option for meeting future energy demands and addressing environmental concerns [62–65]. Therefore, BCN-based photocatalysts have been considered one of the most valuable emerging materials for the fabrication of value-added chemicals and remediation of wastewater. The photodegradation performance of BCN-based catalyst was extensively investigated for methyl orange (MO), rhodamine B (RhB), and tetracycline (TC) removal from waters [66,67].

Balakrishnan et al. [67] studied the fabrication of copper-loaded BCN (Cu-BCN) using a rapid and straightforward technique for the treatment of MO with sonication and solar irradiation. The degradation efficiency improved with loading and reached 94.5% after 15 min for a 10 mg/L loading (cut-off), after which it approached saturation. The degradation efficiency decreased to 52% under relatively neutral conditions but increased to 94.5% under acidic conditions (4–6). Under ultrasonic irradiation, dye degradation in the MO solution increased with the addition of enhancers, such as H_2O_2, and was slowed by scavengers, such as NaCl. Under highly reactive conditions, such as ultrasonic irradiation, additional H_2O_2 decomposes, releasing many reactive OH radicals. In combination with the Cu-BCN interface, these radicals oxidized the MO dye with a degradation efficiency of approximately 96%. In contrast, sonocatalytically produced OH radicals are caught by chloride ions, lowering the degradation efficiency to 62%. In addition, a simple approach based on the availability of a nitrogen atmosphere and a low temperature for fabricating BCN with a bandgap of 3.01 eV was developed to degrade industrial dyes. Compared to C_3N_4, boron improved the thermal stability of the compound by 2%. Moreover, compared to C_3N_4 materials, by which only 86.83% of the dye was degraded, the stacked sheet morphology in BCN improved the effective surface area, increasing the degradation efficiency to 97.53%. Even after 5 cycles of operation, there was only a 7% decline in the catalytic efficiency of BCN [68]. Yan et al. [69] prepared BCN with a pyromellitic dianhydride (BCN-PA) composite for the photodegradation of TC. The TC adsorption capacity of BCN-PA increased from 66.2 to 74.7 mg/g as the pH increased from 3.73 to 6.80. The BCN-PA photodegradation efficiency for TC was also greater at pH 6.80 than at pH 3.73 under visible-light irradiation. Metal-free ceramic BCN nanosheets were used to establish a technique for decarboxylation of carboxylic acids. Isotopic tests revealed that methanol is the hydrogen atom donor, and control experiments suggested a radical reaction [69]. Wang et al. (2021) prepared a Ag_3PO_4/BCN nanocomposite photocatalyst for the removal of organic contaminants such as MO, RhB, and TC under visible light. After exposure to visible light, pure Ag_3PO_4 demonstrated modest photocatalytic activity, degrading 70, 64, and 26% of RhB, TC, and MO, respectively. Compared to the pure Ag_3PO_4 nanoparticles, all Ag_3PO_4/BCN demonstrated increased photocatalytic activity against all contaminants. It not only boosted the photocatalytic effectiveness but also increased the pace at which these pollutants were degraded [70]. For photocatalysis, BCN nanosheets were also synthesized via thermal condensation (TBCN) and the solvothermal route (SBCN). The optical bandgap of TBCN (2.68 eV) is comparable to that of a typical semiconductor. These materials were tested for acid green (AG), MG, and reactive navy blue (RNB) degradation, and TBCN showed better removal efficiency performance, up to 91.3%. Five degradation experiments for the treatment of MG dye were conducted to assess the stability and reusability of TBCN. Under UV irradiation, TBCN (0.2 g/L) was employed for repeated degradation. The effectiveness of the photocatalyst decreased by only 4% from the first cycle after five successive cycles, demonstrating its high stability [27]. Pios et al. [72] used high-level ab initio electronic structure theory to design and analyze triangular BCNs, a family of new heteroaromatic chromophores. These unique heterocycles inherit the inverted singlet-triplet gap from heptazine, and their absorption and luminescence spectra and transition dipole moments are broadly tunable. The color of the emission may change and fluorescence production can be increased for use in OLEDs. In another study, the photoelectrocatalysis method was utilized to examine the degradation of organic contaminants in gas-field-generated water. The electrical conductivity of the wastewater was lowered from 6300 to 1100 μS/cm using a simple evaporation procedure, and the initial COD was reduced from 9500 mg/L to 750 mg/L. The COD of the distilled wastewater from the evaporation process was reduced to 143 mg/L using the photoelectrocatalysis method in a coil-type microreactor. A maximum COD removal of 81% was achieved at an operating time of 15 min, pH = 3, cell voltage of 20 V, electrical conductivity of 2500 μS/cm, and H_2O_2 concentration of 8 mM [71]. A metal-free heterogeneous photocatalytic system including BCN was developed via the facile decarboxylative $C(sp^3)$–$C(sp^2)$ coupling reaction of aryl acetic acids and (hetero)arenes and the substrate generality of $C(sp^3)$–N cross-couplings for direct decarboxylation. A variety of aryl acetic acid substrates containing electron-rich substituents, such as methoxy, methyl, and t-Bu, were easily transported to the required products. The $C(sp^3)$–N coupling of 2-(naphthalen-2-yl) acetic acid with 1-(naphthalen-2-ylmethyl)-1H-pyrazole was also effective. Decarboxylative $C(sp^3)$–N coupling products produced from widely available anti-inflammatory medications, such as naproxen and ibuprofen, were obtained in moderate to good yields of 42–63% [72]. Kumar et al. [74] fabricated Fe@TiO_2/BCN (FT/BCN) for TC removal and CH_4 production. Fig. 1A shows the entire synthetic hydrothermal method for Fe@TiO_2/BCN. An acidic precursor was initially prepared by combining sulfuric acid with 100 mL of pure water. Then, 10 mL of tetrabutyl titanate ($Ti(OC_4H_9)_4$) was dissolved in a separate jar, along with a small quantity of Fe $(NO_3)_3.9H_2O$. An acidic precursor was gradually added to generate a clear yellow TiO_2 precursor solution. Subsequently, a predetermined quantity of BCN was added and sonicated for 30 min. The mixture was then placed in an autoclave and treated hydrothermally for 12 h at 180 °C. The resultant powder was washed multiple times with water and ethanol before being dried. The SEM image of FT30/BCN (Fig. 1B) shows that the spherical Fe@TiO_2 nanoparticles were spread consistently throughout the uneven porous sheet of BCN, and a similar trend was confirmed by TEM image. The proximity of the two is undoubtedly helpful for electron transport and, as a result, for photocatalytic activity. Under visible light, pH significantly affected TC removal, as shown in Fig. 1C. At a pH of 5.4, the maximum TC removal rate was 96.2%. The TC and total organic carbon (TOC) removals under solar and visible light using the FT30/BCN catalyst were also examined. In distilled water (DW) and river water (RW), 84.1 and 81.2% of TC was eliminated in 60 min under natural sunlight, respectively. In DW, high mineralization was also recorded, with 77.2 and 64.3% TOC removal rates at an

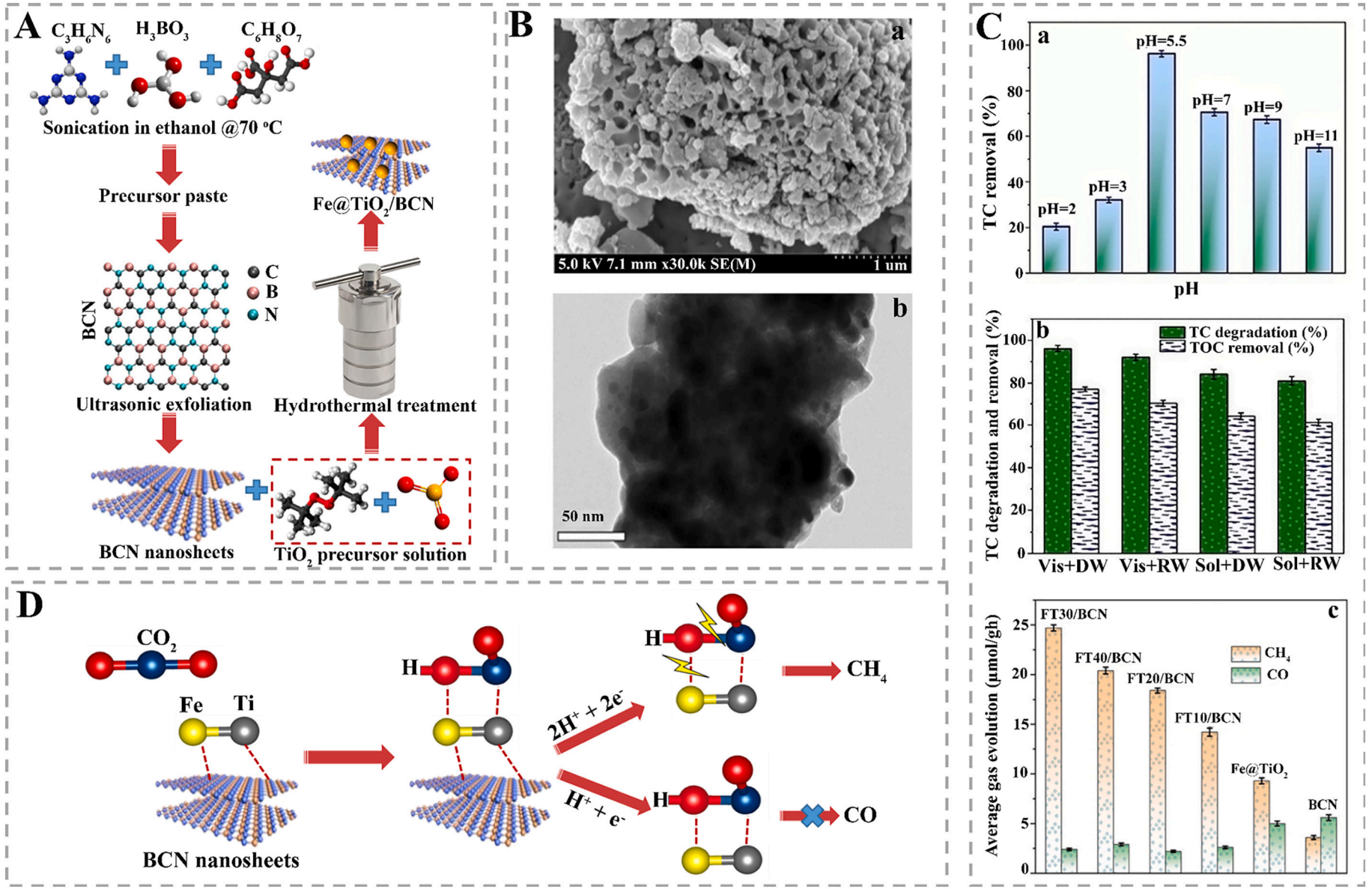

Fig. 1. (A) Fabrication procedure for Fe@TiO_2/BCN material, (B) Morphological structure of Fe@TiO_2/BCN as shown by SEM (a) and TEM (b) images, (C) Tetracycline (TC) removal efficiencies at different pH values (a), TC and total organic carbon (TOC) removal efficiencies with different light sources (b), and CO_2 and CH_4 evolution with different materials (c), and (D) Possible CH_4 evolution mechanism using Fe@TiO_2/BCN. Adapted from Kumar et al. (2022) with permission from Elsevier (license number: 5243581257313).

operating time of 2 h under solar and visible light, respectively. On the other hand, Fig. 1C illustrates the cumulative CH_4 and CO development and the selectivity of several samples. CH_4 evolves in the order FT30/BCN > FT40/BCN > FT20/BCN > FT10/BCN > Fe@TiO_2 > BCN with evolution rates of 24.7, 20.4, 18.4, 14.2, 9.3, and 3.6 μmol/g.h, respectively. Furthermore, FT30/BCN has the highest CH_4 production (91.1%) and the lowest CO evolution (3.6 μmol/g.h). Fig. 1D represents the production of CH_4 in the opposite direction. The presence of Fe@TiO_2 facilitates the formation of two metal sites on the FT30/BCN heterojunction photocatalyst. Consequently, Fe and Ti can connect with C and O atoms simultaneously (in CO_2, as indicated in the image) to generate Fe–C–O–Ti, an M1–C–O–M_2 chemical intermediate that favors only CH_4 production.

3.2. BCN based adsorbents

The most promising and widely used strategy in wastewater treatment operations is the adsorption process, which has low cost, is simple to operate, and has high removal efficiency. Numerous adsorbents have been explored to reduce the contaminant and pollutant concentrations in wastewater. Acid–base, electrostatic, and π–π interactions and hydrogen bonding, porosity, and pore size are the most critical properties of the adsorption process. Therefore, as a new emergent material, BCN exhibits the aforementioned superior properties for application as an adsorbent in the purification of wastewater [73,74]. The adsorption performance of BCN-based adsorbents was extensively performed for dyes [75], heavy metals, and antibiotics [76] removal from waters.

Novel flower stamen-like BCN nanoscrolls with a large surface area of 890 m^2/g were synthesized using a facile method for water purification. They exhibited outstanding dye adsorption capacities of 620 mg/g and 250 mg/g for CR and MB, respectively. After 3 min, 90% of the MB was treated, and there was almost no MB remaining after 10 min, indicating remarkable absorption performance in the elimination of MB. The regeneration of BCN absorbents at a temperature of 400 °C and operating time of 2 h allowed a 93% retention of adsorption activity [12]. Peng et al. [1] developed a one-pot synthesis technique for BCN nanosheets by pyrolyzing a combination of melamine and boric acid to remove heavy metal ions. As a result of synthesizing a range of products by adjusting the molar ratio of boric acid and melamine and the temperature to improve synthesis conditions, BCN nanosheets made from a 3:3 molar ratio at 550 °C were selected as having the greatest Hg^{2+} and Pb^{2+} removal efficiencies. The BCN nanosheets demonstrated promising performance, with highest adsorption capacities of 625.0 and 210.97 mg/g for Hg^{2+} and Pb^{2+}, respectively, due to the effective insertion of numerous functional groups, increased surface sites, and hydrophilicity. The pseudo-second-order kinetic results showed chemisorption, and the sorption isotherms agreed well with the Langmuir model, indicating monolayer adsorption. Furthermore, the BCN nanosheets exhibit high chemical stability, with adsorption capabilities of more than 90% after six adsorption/desorption cycles [1]. Guo et al. [2] developed a BN-CN composite for the treatment of dyes in water. The multilayer BN-CN could efficiently remove NR and MG with capacities of 1350.1 and 1040.6 mg/g from water containing 220 mg/L of NR and 120 mg/L of MG, respectively. MO, MB, and CV were all removed in minor amounts of approximately 60 mg/g at an initial concentration of 120 mg/L. A hydrogel template and freeze-casting approach have been used to create a variety of unique aerogel-like BCNs with porous structures. The ideal BCN aerogel has the highest adsorptive desulfurization (ADS) capacity for aromatic organosulfur compounds (30.8 mg S/g adsorbent), which is much greater than the state-of-the-art aerogel adsorbents reported under comparable circumstances (17.1 mg S/g adsorbent). On the BCN aerogel, DBT adsorption was selective in the presence of aromatic hydrocarbons and nitrogen molecules [77]. In a separate study, NR and MG were removed from aqueous solutions using BCN. A molecular model of BCN mixed with various dyes is shown in Fig. 2A to reveal the possible interactions between the dyes and BCN. Moreover, the adsorption capacities of dyes are illustrated in Fig. 2B. In a NR–MB–MO ternary mixed solution, the BCN adsorption capacity for NR is 628.50 mg/g, whereas the BCN adsorption capacities for MB and MO are 170.8 and 248.4 mg/g, respectively. However, in a MG–MB–MO ternary mixed system, the adsorption capacity of BCN for MG is 612.79 mg/g, whereas the adsorption capacities for MB and MO are 172.05 and 275.51 mg/g, respectively. The BCN adsorption capacities for NR and MG were 641.55 and 597.14 mg/g, whereas they were 318.43 and 384.22 mg/g for MB and MO, respectively. This difference most likely occurs because the high performance of BCN for NR and MG is related to the high affinity of BCN for H^+, whereas the adsorption capacity of BCN for MB and MO is unrelated to the affinity of BCN for H^+. In addition, the release results shown in all the figures demonstrate that BCN may selectively adsorb and quickly release NR and MG from ternary and quaternary mixed

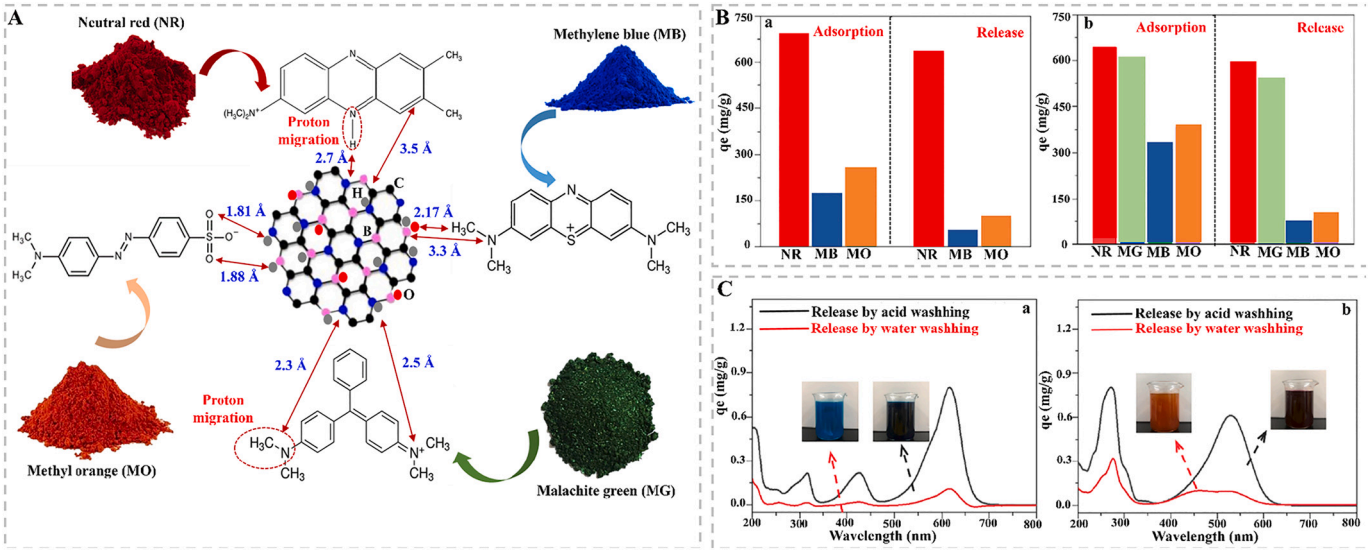

Fig. 2. (A) Molecular based model of BCN with neutral red (NR), methylene blue (MB), malachite green (MG), and methyl orange (MO), (B) The NR, MB, and MO dye adsorption–desorption capacities of BCN from ternary mixed solution (a) and the MG, MB, and MO dye adsorption–desorption capacities of BCN from ternary mixed solution (b), and (C) The absorbance peaks of MB dye (a) and NR dye (b) released from BCN using water and acid washing. Adapted from Luo et al. [77] with permission from Elsevier (license number: 5243590991643).

solutions of NR, MG, MB, and MO. In addition, the peak of MB dye released by acid washing (Fig. 2C) was more significant than the peak of MB dye released by water washing, demonstrating that lowering the pH of the solution efficiently released the MB dye adsorbed by BCN. The color of the BCN solution obtained by acid washing was substantially darker than the color of the BCN solution obtained by water washing. Water washing resulted in the release of 105.21 mg/g of MB dye, whereas acid desorption resulted in the release of 631.54 mg/g of MB dye from the BCN material [78].

Various forms of BCN synthesized via thermal polymerization of urea during the calcination process, annealing mixtures of poly (ethylene oxide-*co*-propylene oxide) (P123), boric acid, and urea, and oxygen-limited methods have been used for the removal of organic dyes such as NR, MG, MO, MB, CR, and CV from water (Table 1). Layered BN-CN with a surface area of 132.16 m^2/g had 1350.1 and 1040.6 mg/g sorption capacities for NR and MG, respectively, and ~a 60 mg/g capacity for MO, MB, and CV, respectively. The Langmuir isotherm was the best fit isotherm for dye adsorption behavior, followed by pseudo-second-order kinetics. On the other hand, the BCN nanoscrolls exhibited adsorption capacities of 620 mg/g for CR and 250 mg/g for MB. In addition, an aerogel-like BCN engineered using a hydrogel template and freeze-casting was utilized for the desulfurization of water containing 500 mg/L of sulfur. The material having a surface area of 1220 m^2/g produced a sulfur sorption capacity of 30.8 mg/g, which was well described by the Langmuir–Freundlich combined model. Moreover, TC removal from water with an initial concentration of 40 mg/L was carried out using BCN synthesized by an oxygen-limited method and a 76.74 mg/g adsorption capacity was reported. Additionally, pH-responsive BCN also prepared via an oxygen-limited method employed for dye removal from aqueous solutions and showed lower adsorption capacities, such as 747.10 mg/g for NR, 682.46 mg/g for MG, 61.27 mg/g for MO, and 119.38 for MB, than layered BN-CN synthesized by thermal polymerization of urea during the calcination process. The adsorptive behavior of the pH-responsive BCN for dye removal was defined by the Langmuir model, and its kinetics obeyed the pseudo-second-order model.

3.3. BCN in electrochemical reduction

BCN is an environmentally friendly and cost-efficient emerging material that has recently been used in wastewater and water treatment. The simultaneous removal of nitrate and production of ammonia from wastewater using the electrochemical reduction method with BCN has attracted significant scientific attention. Reportedly, industrial ammonia generation is still based on the energy-intensive Haber–Bosch method, which operates under severe conditions (temperature of 300–550 °C and pressure of 150–250 atm). Moreover, the hydrogen used in this method originates from natural gas (NG) cracking, which consumes energy and emits CO_2. Therefore, researchers have focused on the use of electrochemical processes for the reduction of nitrate to ammonia using noble metals such as Au, Ag, Ru, and Rh [80–83]. Moreover, the nitrate reduction performance of linked heterostructure metal-free boron, carbon, phosphorus, and sulfur has also been investigated [84,85]. Nevertheless, the use of these noble metals in real-scale applications is limited because of their scarcity and high price [86]. The low ammonia production and Faraday efficiency (FE) values of cost-effective metal-free catalysts indicate a need for effective catalysis in electrochemical nitrate reduction [87,88]. Therefore, researchers have initiated the development of metal-organic heterostructure materials to enhance ammonia production through their polarization and charge separation effects between organic compounds and metals.

Several studies have been conducted on metal-solidified BCN

Table 1
Summary of the published studies on water treatment with BCN nanosheets as an adsorbent.

Adsorbent	Synthesis method	Surface area (m^2/g)	Adsorption capacity (mg/g)	Isotherm constant	Kinetic rate constant	Adsorption conditions	Reference
Layered BN-CN composite	Thermal polymerization of urea during the calcination process	132.16	1350.1 (C_0 = 220 mg NR/L) 1040.6 (C_0 = 120 mg MG/L) ~60 (C_0 = 120 mg MO/L) ~60 (C_0 = 120 mg MB/L) ~60 (C_0 = 120 mg CV/L)	0.388^{L}	0.00026^{PSO}	Adsorbent dose: 0.09 g/L; T = 25 °C; pH = 6.66; Equilibrium time: 8 h	[2]
BCN nanoscrolls	Annealing mixtures of poly(ethylene oxide-*co*-propylene oxide) (P123), boric acid and urea	890	620 (C_0 = 110 mg CR/L) 250 (C_0 = 80 mg MB/L)	$N.A.^{L}$	N.A.	N.A.	[12]
Aerogel-like BCN	Hydrogel template and freeze casting	1220	30.8 (C_0 = 500 mg sulfur/L)	0.0013^{LF}	N.A.	Adsorbent dose: 2.5 g/L; T = 25 °C; Equilibrium time: 3 h	[77]
BCN nanosheets	Pyrolysis of a mixture of melamine and boric acid	55.7	625 (C_0 = 307.8 mg Hg^{2+}/L) 210.97 (C_0 = 108 mg Pb^{2+}/L)	1.039^{L} 1.411^{L}	6.148×10^{-4} PSO 9.27×10^{-2} PSO	Adsorbent dose: 0.4 g/L; T = 25 °C; pH = 7; Equilibrium time: 40 min	[1]
BCN	Oxygen-limited	18.708	76.74 (C_0 = 40 mg Tetracycline/L)	0.27^{L}	0.0010^{PSO}	Adsorbent dose: 0.4 g/L; T = 25 °C; pH = 7.87; Equilibrium time: >210 min	[79]
pH-responsive BCN	Oxygen-limited	N.A.	747.10 (C_0 = 150 mg NR/L) 682.46 (C_0 = 150 mg MG/L) 61.27 (C_0 = 150 mg MO/L) 119.38 (C_0 = 150 mg MB/L)	$N.A.^{L}$	$N.A.^{PSO}$	Adsorbent dose: 0.2 g/L; Equilibrium time: 240 min	[78]

BN-CN: Boron nitride-carbon nitride, BCN: Boron carbon nitride, NR: Neutral red, MG: Malachite green, MO: Methyl orange, MB: Methylene blue, C_0: Initial pollutant concentration, CV: Crystal violet, CR: Congo red, N.A: Not available, L: Langmuir isotherm (KL, L/mg), F: Freundlich isotherm (KF), T: Temperature, LF: Langmuir–Freundlich (KLF, (L/mg)n), PFO: Pseudo-first order (k1, min^{-1}), PSO: Pseudo second-order (k_2, g/mg·min).

catalysis for ammonia production via electrochemical reduction. Zhao et al. [72] studied the electrochemical reduction of dinitrogen to produce ammonia using a Ni-doped BCN catalyst (BCN@Ni). The highest ammonia generation rate of 16.7 μg/hcm^2 and FE of 13.1% were obtained at an applied potential of 0.3 V and operating time of 12 h. Moreover, the reusability studies of BCN@Ni showed that its activity and stability persisted after 8 cycles. To enhance ammonia production, Zhao et al. [73] also synthesized copper (Cu) nanoparticles embedded in a vesicle-like BCN (BCN@Cu) by processing a metal–boron organic polymer precursor at a temperature of 1000 °C. The novel BCN@Cu was used to convert nitrate to valuable ammonia in water, and the results revealed that the BCN@Cu has significant catalytic activity for electrochemical nitrate reduction. The effect of the applied potential (0.3–0.6 V) on ammonia yield and FE was investigated, and the results showed that the ammonia yield increased with increasing applied potential. The highest ammonia yield of 576.2 μmol/h.mg.cat with an FE of 88.9% was obtained at an applied potential of 0.6 V, while the lowest ammonia yield of 271.1 μmol/h.mg.cat with an FE of 86.3% was obtained at the potential of 0.3 V. Moreover, according to isotopic labeling experiments, they reported that the ammonia production was derived from the electrochemical reduction of nitrate onto the BCN@Cu surface. Overall, these results revealed that the presence of Cu in BCN@Cu is the most critical factor affecting nitrate reduction activity. In contrast, the presence of B can significantly enhance the reduction properties of BCN@Cu by supporting the distribution of Cu nanoparticles within BCN, thereby increasing the active surface area available for nitrate reduction. In a separate study, the production of valuable ammonia from the treatment of nitrate in sewage wastewater using an electrochemical reduction method with nickel (Ni) nanoparticles and single-atom Ni on BCN (BCN@Ni-Ni) as an electrode was investigated [91]. The effects of water media (0.1 M phosphate buffer: pH 7, 0.1 M KOH, pH 13, and 0.1 M HCl: pH 1) on ammonia production rate were investigated. The highest ammonia production rate of 1706.0 μmol/h.mg.cat and FE of 91.2% were obtained in alkaline media at an applied potential of 0.5 V, whereas the lowest ammonia production rate of 1400.1 μmol/h.mg.cat and FE of 68.2% were observed in neural media. Moreover, reusability studies of the BCN@Ni catalyst showed that the activity of the catalyst was sustained after 10 cycles or an operating time of 20 h. Zhao et al. [75] also synthesized single-atom Cu with BCN on CNTs (BCN@Cu/CNT) to treat nitrate and produce value-added ammonia simultaneously from sewage via an electrochemical reduction process. The preparation method for the BCN@Cu/CNT catalyst is presented in Fig. 3A. Moreover, based on the elemental mapping results collected from a TEM image, B, C, Cu, and N were observed on the catalyst surface. XPS analysis was performed to discern the valance and possible bonds of the elements onto the BCN@Cu/CNT catalyst surface. The results showed that the highest binding energy of 933.6 eV was observed for CuO, whereas the binding energies for zero-valent Cu and Cu $2p_{3/2}$ were 932.4 and 932.8 eV, respectively, which indicated that the catalyst surface consists of Cu with a valence of 0–2^+ (Fig. 3B). The peaks at binding energies of 189.4, 190.7, and 192.2 eV indicate B—C, B—N, and B—O bonds of B element, respectively. The highest binding energy of 284.5 eV was obtained for sp_2 C originating from graphitized C in CNT, and C—N and C═O bonds with binding energies of 284.4 and 290.2 eV were also observed for C. In addition, N element was formed due to the pyrolysis of MBOP/CNT, and N peaks in the catalyst showed N—B, pyridinic–N, N—C, and pyrrolic–N bonds with binding energies of 397.8, 399.0, 400.0, and 401.5 eV, respectively. The surface morphology of the catalyst was investigated using scanning electron microscopy (SEM), and the images showed that BCN@Cu was effectively adsorbed onto the CNT, resulting in a homogenous nanotube shape BCN@Cu/CNT (Fig. 3C). Transmission electron microscopy (TEM) results also showed that high-contrast bright spots on the catalyst surface, which most probably represent single-atom Cu signals, were apparent at the 5 nm scale field of view. A nickel foam electrode (2 × 2 cm) was coated with the synthesized BCN@Cu/CNT catalyst to treat low-nitrate content water (50 mg/L). The effect of electrolytic current (10–50 mA) on nitrate removal efficiency was investigated, and the results showed that the highest removal efficiencies of 54.7, 89.2, and 99.3% occurred under electrolytic currents of 10, 30, and 50 mA, respectively, at an operating time of 5 h (Fig. 3D). Moreover, the ammonia production from the treatment of nitrate with the electrochemical reduction process using the BCN@Cu/CNT catalyst revealed that the ammonia production efficiency was almost 10% in the treatment of 50 mg/L of nitrate-containing wastewater at an operating time of 1 h (Fig. 3D). The reusability of BCN@Cu/CNT was also studied, and the nitrate removal efficiency and ammonia production were >95.8 and 11.0%, respectively, at the end of the 10 cycles and an operating time of 5 h. To summarize the above-mentioned results, the possible nitrate removal and ammonia production pathways of BCN@Cu/CNT under different nitrate concentrations and electrolytic currents are illustrated in Fig. 3E.

Overall, the above-mentioned studies revealed that BCN nanosheets have been widely utilized in electrochemical processes for simultaneous nitrate treatment of water and ammonia production from water. The features of the BCN nanosheets, treated water types, and optimum operating conditions are summarized in Table 2. Moreover, the value-added product formation yields and FE values under optimized conditions for different BCN nanosheets are also presented. Cu and Ni have been used to enhance the electrochemical nitrate reduction performance of BCN materials. The results revealed that the removal and production of metal-loaded BCN nanosheets were higher than those of metal-free BCN nanosheets because of their high surface area, high stability, and effective reduction activity. For example, the highest ammonia production of 172,226.5 μg/h.mg.cat and FE of 95.3% were obtained using the BCN@Cu/CNT catalyst, while the ammonia production and FE values were 7.75 μg/h.mg.cat and 13.8% for metal-free BCN. The minimum FE was also 13.1% using BCN@Ni since partial electron transfer from nano-Ni particles to BCN suppresses the hydrogen evolution process and reduces the rate-determining step on Ni surfaces toward nitrogen reduction reaction. These results proved that the interaction between the BCN matrix and Ni nanoparticles supports a synergetic effect for electrochemical nitrogen reduction reaction efficiency and FE. As a result, by modifying the electrical characteristics of non-noble metals via the development of a hetero-interface, efficient performance and FE may be attained. Furthermore, the effect of the loaded metal on the performance of BCN was investigated, and the results revealed that the ammonia production rate using Cu-loaded BCN nanosheets was almost 338 times higher than that using Ni metal-loaded BCN nanosheets. The maximum ammonia production was reported to be 576,200 μmol/h.mg.cat with an FE of 88.9% and 1706.0 μmol/h.mg.cat with an FE of 91.2% for the BCN@Cu and BCN@Ni-Ni nanosheets, respectively. Similarly, the ammonia production rate of BCN-Ni nanosheets was 16.72 μg/hcm^2 with FE of 13.1%, while it was 3358.74 μg/hcm^2 with FE of 97.4% for two-dimensional Cu loaded BCN nanosheets. Moreover, the reusability experiments showed that the activity and stability of BCN-Ni were sustained for 10 cycles, while the reduction activity of BCN-Cu nanosheets continued for 8 cycles.

3.4. Other processes

Several treatment technologies have been developed for water desalination, including reverse osmosis (RO) [94], microbial desalination cells (MDCs) [95], electrocoagulation [96], capacitive deionization (CDI) [97], and electrodialysis [34,98,99]. Nevertheless, disadvantages such as the formation of chemical sludge, high operational costs, excessive use of chemicals, membrane scaling and fouling, and high electrical energy consumption, either individually or as a combination, hamper effective use of these technologies. The CDI process has received considerable attention owing to its significant benefits such as environmental friendliness, ease of operation, and low energy consumption [100,101]. Research has been widely focused on the development of effective electrode materials because they have a significant effect on

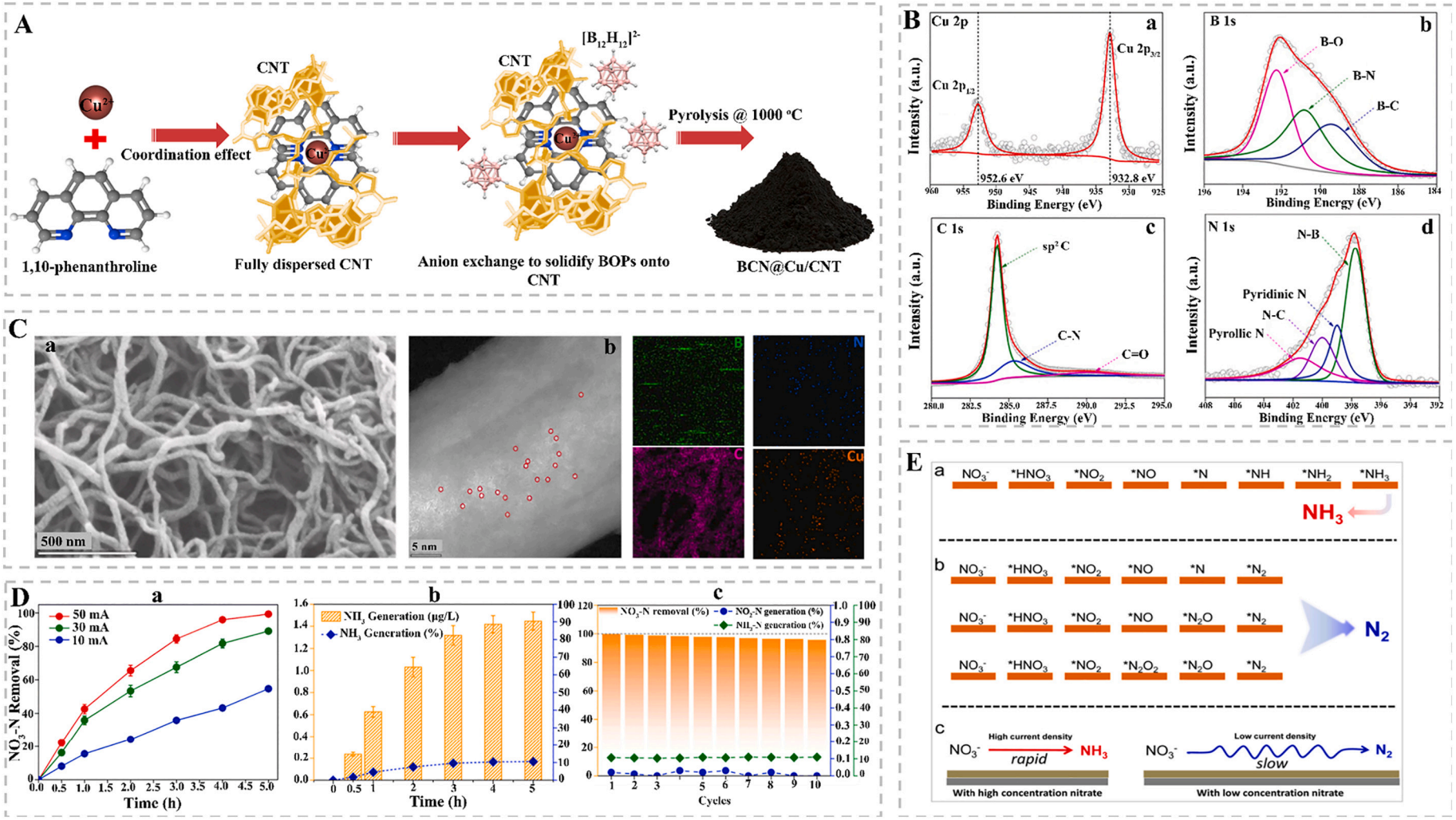

Fig. 3. (A) Synthesis procedure for BCN@Cu/CNT material, (B) XPS results for Cu metal in BCN@Cu/CNT (a), XPS results for B metal in BCN@Cu/CNT (b), XPS results for C element (c), and XPS results for N element (d), (C) Morphological structure of BCN@Cu/CNT by SEM (a) and TEM images and elemental mapping of BCN@Cu/CNT (b), (D) Nitrate removal efficiency of material at different applied potential (a), Ammonia generation performance of material (b), and Reusability performance of material (c), and (E) Possible pathways for removal of nitrate and production of ammonia. Adapted from Zhao et al. (2022) with permission from Elsevier (license number: 5243590991643).

Table 2
Summary of the literature studies on treatment of water with BCN nanosheets in electrochemical reduction processes.

Catalyst type	Loaded metal	Water source	Optimum conditions	Ammonia yield rate	Faradic efficiency (%)	Reusability performance (cycle)	Reference
BCN@Cu/CNT	Cu	SS	Initial nitrate concentration: 100 mM; Applied potential: 0.6 V; Operating time: 5 h	172,226.5 μg/h.mg.cat.	95.3	10	[92]
BCN@Ni	Ni	SS	Applied potential: 0.3 V; Operating time: 2 h	16.72 μg/h.cm^2	13.1	8	[89]
BCN@Cu	Cu	SS	Initial nitrate concentration: 100 mM; Applied potential: 0.6 V; Operating time: 1 h	576,200 μmol/h.mg.cat.	88.9	10	[90]
BCN@Ni-Ni	Ni	SS	Initial nitrate concentration: 100 mM; Applied potential: 0.5 V; pH: 13; Operating time: 1 h	1706.0 μmol/h.mg.cat	91.2	10	[91]
2D BCN@Cu	Cu	SS	Initial nitrate concentration: 100 mM; Applied potential: 0.6 V; Operating time: 1 h	3358.74 μg/h.cm^2	97.4	10	[93]
BCN	–	SS	Initial nitrogen concentration: 99.9% N_2 gas with flow rate of 10 mL/min; Applied potential: 0.3 V; Operating time: 2 h	7.75 μg/h.mg.cat.	13.8	–	[87]

BCN: boron carbon nitride, BCN@Cu/CNT: Cu-loaded BCN on carbon nanotube, BCN@Ni: Ni-doped BCN, SS: synthetic solution, 2D: two-dimensional.

the performance assessment of CDI [102,103]. Activated carbon, carbon aerogels, carbon nanotubes, carbon spheres, and graphene materials are extensively preferred in CDI because of their high conductivity, good stability and activity, and high surface area [104–107]. However, the low adsorption performance and high synthesis cost of these materials have forced researchers to develop novel carbon-based electrode materials [108,109]. Owing to their unique features, BCN nanosheets have been extensively studied in the fields of batteries [110], catalysis [71,111], absorption [112], and supercapacitors [113]. Since carbon-based supercapacitors and CDI processes have a similar principle, BCN could be suitable for CDI electrodes owing to its superior capacitive efficiency [114–116]. However, to the best of our knowledge, because the use of BCN to enhance treatment processes is a topic of study that has recently gained a great deal of interest, there is only one study in which this material was employed in the CDI process as an electrode material.

Wang et al. [117] fabricated novel BCN nanosheet electrodes using boric acid as a boron source and g-C_3N_4 as both a nitrogen source and a template for water desalination in the CDI process. The highest adsorption capacity of 13.6 mg/g was achieved at an applied potential of 1.4 V and initial NaCl concentration of 500 mg/L. Moreover, the stability and activity of the BCN electrode were investigated, and the results revealed that the electrode showed considerable stability after 15 cycles. Overall, the results indicated that BCN nanosheets could be a feasible option for effective CDI electrode performance.

4. Conclusions and perspective

In this review, studies on water and wastewater treatment using BCN-integrated treatment processes are summarized and discussed. The fabrication methods for BCN nanosheets, chemical and physical properties of BCN, optimization of BCN production with different metals, morphological characteristics of BCN, and wastewater treatment performance were evaluated. Moreover, the benefits and drawbacks of using BCN in treatment processes for simultaneous wastewater removal and value-added product generation were reviewed.

In electrochemical reduction processes, BCN nanosheets are used as electrode materials for nitrate removal during the production of ammonia from wastewater. Cu and Ni were loaded onto the surface of the BCN to enhance their performance. The maximum ammonia production rate was 1706.0 μmol/h.mg.cat with an FE of 91.2% was achieved using the BCN@Ni catalyze in a 0.1 M KOH solution at an applied potential of 0.5 V. Furthermore, the stability and activity of the BCN@Ni catalyst were sustained after 10 cycles for an operating time of 20 h. On the other hand, the lowest ammonia production rate of 576.2 μmol/h.mg.cat with an FE of 88.9% was obtained at an applied potential of 0.6 V using BCN@Cu catalyze. These results show that the presence of Ni in BCN@Ni increased the active surface area available for nitrate reduction compared to Cu-metal-loaded BCN catalysts. In addition, the removal of organic compounds, dyes, and TC from water resources using BCN-based photocatalysts has been widely performed. The highest dye removal efficiencies of Cu-metal-loaded BCN and metal-free BCN nanosheets as effective photocatalysts were in the range of 94.5–97.5% as an effective photocatalyst. For TC removal, the maximum removal efficiency was 96.2%, with a CH_4 production efficiency of 91.1% using Fe@TiO_2/BCN and 95.0% using the BCN-PA photocatalyst. The highest COD removal efficiency was reported to be 85.0% using a metal-free BCN photocatalyst at an operating time of 15 min, pH of 3, applied potential of 20 V, conductivity of 2500 μS/cm, and H_2O_2 concentration of 8 mM.

Moreover, BCN-based materials have been used as adsorbents for the removal of heavy metals, dyes, and organosulfur compounds from wastewaters. A maximum MD dye removal efficiency of 100% at an operating time of 10 min was achieved using BCN nanoscrolls. The adsorption-desorption experiments of adsorbent also revealed that the BCN adsorption capacity remained at 93% after thermal treatment at a temperature of 400 °C for 2 h. For heavy metal removal, the highest adsorption capacities of the BCN nanosheets were 210 and 625 mg/g for Pb^{2+} and Hg^{2+}, respectively. Reusability experiments of BCN after metal removal also showed that the adsorbent activity was over 90% after 6 cycles. Moreover, a single study was conducted on water desalination using BCN nanosheets as the electrode material in the CDI process. The maximum salt adsorption capacity of 13.6 mg/g was obtained at an initial NaCl concentration of 500 mg/L and a potential of 1.4 V. Based on the above-mentioned studies, it can be concluded that the utilization of BCN nanosheets directly or integrated with other processes is a promising option for the effective removal of contaminants from water.

Overall, the high adsorption capacity and removal efficiency, enhanced regeneration ability, stable electrochemical activity, low cost, ease of fabrication and operation, and environmental sensitivity of BCN nanosheets for wastewater treatment suggest promising prospects for domestic and industrial applications, including the green production of value-added products such as ammonia and methane. Moreover, these materials do not show harmful impacts on humans and the environment, and thus they are believed to be environmentally friendly owing to their green synthesis, stability against aggregation in water, and low toxicity. This review paper revealed that BCN nanosheets could be used effectively in wastewater and water treatment and in common areas such as biosensors, batteries, and capacitors. This study also showed that BCN nanosheets have been used in wastewater treatment recently, revealing a large room for new studies on this subject. There is a considerable need for further research on wastewater treatment using BCN nanosheets to understand the limitations and benefits of these materials in accurate scale applications, as this field of research is novel. For instance, metals, such as Cu and Ni, are generally used to increase the performance of BCN nanosheets. These results promote the exploration of different metals and development of new synthesis methods to realize the complementary advantages of BCN nanosheets. Furthermore, leaching the loaded metals should be considered to enhance materials' applicability on a real scale. To our best knowledge, there is little research on real wastewater

treatment in the presence of several pollutants using BCN nanosheets. However, the experiments should be performed by mimicking real wastewater to understand the combined effects of contaminants on BCN removal performance. The most crucial gap in the literature is that the studies have been performed on a lab scale. Therefore, further pilot and real-scale applications should be conducted. Moreover, the leaching of metals incorporated with BCN may cause environmental problems in water media. Therefore, the fixation of metallic groups in the BCN can be a novel interest of research to prevent such risks to the environment. Overall, the cost assessment, environmental effects, and human and ecological health risks of the produced materials should be studied in future research to achieve a realistic perspective on applicability on an industrial scale.

CRediT authorship contribution statement

Yasar Kemal Recepoglu: Writing – Original Draft, Methodology, Investigation; **Aysegul Yagmur Goren**: Writing – Original Draft, Investigation, Visualization; **Vahid Vatanpour**: Literature review, Writing – Review & Editing; **Yeojoon Yoon**: Writing – Review & Editing, Designing; **Alireza Khataee**: Literature review, Supervision, Writing – Review & Editing.

Declaration of competing interest

We would like to confirm that there is no known conflict of interest associated with this publication.

Acknowledgements

Y. Yoon acknowledges the supports provided by the National Research Foundation of Korea (NRF) grant funded by the Korea government (MSIT) (No. NRF-2020R1F1A1076312).

References

[1] D. Peng, W. Jiang, F.-F. Li, L. Zhang, R.-P. Liang, J.-D. Qiu, One-pot synthesis of boron carbon nitride nanosheets for facile and efficient heavy metal ions removal, ACS Sustain. Chem. Eng. 6 (2018) 11685–11694.
[2] Y. Guo, R. Wang, P. Wang, L. Rao, C. Wang, Developing a novel layered boron nitride-carbon nitride composite with high efficiency and selectivity to remove protonated dyes from water, ACS Sustain. Chem. Eng. 7 (2019) 5727–5741.
[3] H. Zhang, X. Han, H. Yu, Y. Zou, X. Dong, Enhanced photocatalytic performance of boron and phosphorous co-doped graphitic carbon nitride nanosheets for removal of organic pollutants, Sep. Purif. Technol. 226 (2019) 128–137.
[4] S. Manan, M.W. Ullah, M. Ul-Islam, O.M. Atta, G. Yang, Synthesis and applications of fungal mycelium-based advanced functional materials, J. Bioresour. Bioprod. 6 (2021) 1–10.
[5] J. Shao, Y. Ni, L. Yan, Oxidation of furfural to maleic acid and fumaric acid in deep eutectic solvent (DES) under vanadium pentoxide catalysis, J. Bioresour. Bioprod. 6 (2021) 39–44.
[6] N. Nasrollahi, L. Ghalamchi, V. Vatanpour, A. Khataee, Photocatalytic-membrane technology: a critical review for membrane fouling mitigation, J. Ind. Eng. Chem. 93 (2021) 101–116, https://doi.org/10.1016/j.jiec.2020.09.031.
[7] Y. Hao, S. Wang, Y. Shao, Y. Wu, S. Miao, High-energy density Li-ion capacitor with layered SnS2/reduced graphene oxide anode and BCN nanosheet cathode, Adv. Energy Mater. 10 (2020), 1902836.
[8] D. Chen, X. Hu, Y. Huang, Y. Qian, D. Li, Facile fabrication of nanoporous BCN with excellent charge/discharge cycle stability for high-performance supercapacitors, Mater. Lett. 246 (2019) 28–31.
[9] K. Gopalakrishnan, K. Moses, A. Govindaraj, C.N.R. Rao, Supercapacitors based on nitrogen-doped reduced graphene oxide and borocarbonitrides, Solid State Commun. 175 (2013) 43–50.
[10] I.C. Nnaemeka, O. Maxwell, A.O. Christain, Optimization and kinetic studies for enzymatic hydrolysis and fermentation of colocynthis vulgaris Shrad seeds shell for bioethanol production, J. Bioresour. Bioprod. 6 (2021) 45–64.
[11] P. Giusto, D. Cruz, T. Heil, N. Tarakina, M. Patrini, M. Antonietti, Chemical vapor deposition of highly conjugated, transparent boron carbon nitride thin films, Adv. Sci. 8 (2021), 2101602.
[12] J. Wang, J. Hao, D. Liu, S. Qin, C. Chen, C. Yang, Y. Liu, T. Yang, Y. Fan, Y. Chen, Flower stamen-like porous boron carbon nitride nanoscrolls for water cleaning, Nanoscale 9 (2017) 9787–9791.
[13] X. Ren, C. Chen, M. Nagatsu, X. Wang, Carbon nanotubes as adsorbents in environmental pollution management: a review, Chem. Eng. J. 170 (2011) 395–410.
[14] S. Angizi, M.A. Akbar, M. Darestani-Farahani, P. Kruse, Two-dimensional boron carbon nitride: a comprehensive review, ECS J. Solid State Sci. Technol. 9 (2020) 83004.
[15] Z.F. Zhou, I. Bello, M.K. Lei, K.Y. Li, C.S. Lee, S.T. Lee, Synthesis and characterization of boron carbon nitride films by radio frequency magnetron sputtering, Surf. Coat. Technol. 128 (2000) 334–340.
[16] S. Thomas, M.S. Manju, K.M. Ajith, S.U. Lee, M.A. Zaeem, Strain-induced work function in h-BN and BCN monolayers, Phys. E Low-Dim. Syst. Nanostruct. 123 (2020), 114180.
[17] S. Nakano, M. Akaishi, T. Sasaki, S. Yamaoka, Segregative crystallization of several diamond-like phases from the graphitic BC2N without an additive at 7.7 GPa, Chem. Mater. 6 (1994) 2246–2251.
[18] Y. Zhang, Z. Zhou, Y. Shen, Q. Zhou, J. Wang, A. Liu, S. Liu, Y. Zhang, Reversible assembly of graphitic carbon nitride 3D network for highly selective dyes absorption and regeneration, ACS Nano 10 (2016) 9036–9043.
[19] Q. Cai, S. Mateti, W. Yang, R. Jones, K. Watanabe, T. Taniguchi, S. Huang, Y. Chen, L.H. Li, Boron nitride nanosheets improve sensitivity and reusability of surface-enhanced Raman spectroscopy, Angew.Chem. 128 (2016) 8545–8549.
[20] W. Lei, D. Liu, Y. Chen, Highly crumpled boron nitride nanosheets as adsorbents: scalable solvent-less production, Adv. Mater. Interfaces 2 (2015), 1400529.
[21] H. Karimi-Maleh, F. Karimi, L. Fu, A.L. Sanati, M. Alizadeh, C. Karaman, Y. Orooji, Cyanazine herbicide monitoring as a hazardous substance by a DNA nanostructure biosensor, J. Hazard. Mater. 423 (2022), 127058. https://doi.org/10.1016/j.jhazmat.2021.127058.
[22] H. Karimi-Maleh, A. Khataee, F. Karimi, M. Baghayeri, L. Fu, J. Rouhi, C. Karaman, O. Karaman, R. Boukherroub, A green and sensitive guanine-based DNA biosensor for idarubicin anticancer monitoring in biological samples: a simple and fast strategy for control of health quality in chemotherapy procedure confirmed by docking investigation, Chemosphere (2022), 132928, https://doi.org/10.1016/j.chemosphere.2021.132928.
[23] W. Lei, D. Portehault, R. Dimova, M. Antonietti, Boron carbon nitride nanostructures from salt melts: tunable water-soluble phosphors, J. Am. Chem. Soc. 133 (2011) 7121–7127.
[24] K. Yuge, Phase stability of boron carbon nitride in a heterographene structure: a first-principles study, Phys. Rev. B 79 (2009), 144109.
[25] H. Li, S. Zhu, M. Zhang, P. Wu, J. Pang, W. Zhu, W. Jiang, H. Li, Tuning the chemical hardness of boron nitride nanosheets by doping carbon for enhanced adsorption capacity, ACS Omega 2 (2017) 5385–5394.
[26] M. Kaur, K. Singh, I. Chauhan, R.K. Sharma, A. Vij, A. Kumar, Defects-induced transition in low-temperature electrical properties of boron carbon nitride thin films, J. Mater. Sci. Mater. Electron. 1–9 (2022).
[27] K. Sivaprakash, M. Induja, P. Gomathipriya, S. Karthikeyan, S.T. Umabharathi, Single-step synthesis of efficient nanometric boron carbon nitride semiconductor for photocatalysis, Mater. Res. Bull. 134 (2021), 111106.
[28] K. Nasrin, V. Sudharshan, K. Subramani, M. Karnan, M. Sathish, In-situ synergistic 2D/2D MXene/BCN heterostructure for superlative energy density supercapacitor with super-long life, Small 18 (2022) 2106051.
[29] A. Bafekry, M. Naseri, M.M. Fadlallah, I. Abdolhosseini Sarsari, M. Faraji, A. Bagheri Khatibani, M. Ghergherehchi, D. Gogova, A novel two-dimensional boron–carbon–nitride (BCN) monolayer: a first-principles insight, J. Appl. Phys. 130 (2021), 114301.
[30] S.D. Nehate, A.K. Saikumar, A. Prakash, K.B. Sundaram, A review of boron carbon nitride thin films and progress in nanomaterials, Mater. Today Adv. 8 (2020), 100106.
[31] H. Zhang, K. Wu, E. Jiao, Y. Liu, J. Shi, M. Lu, Self-assembled supramolecule for synthesizing highly thermally conductive cellulose/carbon nitride nanocomposites with improved flame retardancy, J. Colloid Interface Sci. 608 (2022) 2560–2570.
[32] W.L. Kebede, D.-H. Kuo, F.T. Bekena, L.W. Duresa, Highly efficient In–Mo (O, S) 2 oxy-sulfide for degradation of organic pollutants under visible light irradiation: an example of photocatalyst on its dye selectivity, Chemosphere 254 (2020), 126823.
[33] M. Hasanpour, M. Hatami, Photocatalytic performance of aerogels for organic dyes removal from wastewaters: review study, J. Mol. Liq. 309 (2020), 113094.
[34] E.B. Azimi, A. Badiei, J.B. Ghasemi, Efficient removal of malachite green from wastewater by using boron-doped mesoporous carbon nitride, Appl. Surf. Sci. 469 (2019) 236–245.
[35] Y. Wang, G. Chen, H. Weng, L. Wang, J. Chen, S. Cheng, P. Zhang, M. Wang, X. Ge, H. Chen, Carbon-doped boron nitride nanosheets with adjustable band structure for efficient photocatalytic U (VI) reduction under visible light, Chem. Eng. J. 410 (2021), 128280.
[36] M. Zhou, S. Wang, P. Yang, C. Huang, X. Wang, Boron carbon nitride semiconductors decorated with CdS nanoparticles for photocatalytic reduction of CO2, ACS Catal. 8 (2018) 4928–4936.
[37] C. Huang, C. Chen, M. Zhang, L. Lin, X. Ye, S. Lin, M. Antonietti, X. Wang, Carbon-doped BN nanosheets for metal-free photoredox catalysis, Nat. Commun. 6 (2015) 1–7.
[38] M.D. Esrafili, N. Saeidi, Carbon-doped boron nitride nanosheet as a promising catalyst for N2O reduction by CO or SO2 molecule: a comparative DFT study, Appl. Surf. Sci. 444 (2018) 584–589.
[39] W. Liu, T. Yanase, T. Nagahama, T. Shimada, Synthesis of carbon-doped boron nitride nanosheets and enhancement of their room-temperature ferromagnetic properties, J. Alloys Compd. 792 (2019) 1206–1212.
[40] L. Chen, M. Zhou, Z. Luo, M. Wakeel, A.M. Asiri, X. Wang, Template-free synthesis of carbon-doped boron nitride nanosheets for enhanced photocatalytic hydrogen evolution, Appl. Catal. B Environ. 241 (2019) 246–255.

[41] F. Guo, P. Yang, Z. Pan, X. Cao, Z. Xie, X. Wang, Carbon-doped BN nanosheets for the oxidative dehydrogenation of ethylbenzene, Angew.Chem. 129 (2017) 8343–8347.

[42] Z. Liu, M. Zhang, H. Wang, D. Cang, X. Ji, B. Liu, W. Yang, D. Li, J. Liu, Defective carbon-doped boron nitride nanosheets for highly efficient electrocatalytic conversion of N2 to NH3, ACS Sustain. Chem. Eng. 8 (2020) 5278–5286.

[43] X. Li, X. Hao, M. Zhao, Y. Wu, J. Yang, Y. Tian, G. Qian, Exfoliation of hexagonal boron nitride by molten hydroxides, Adv. Mater. 25 (2013) 2200–2204.

[44] L. Niu, J.N. Coleman, H. Zhang, H. Shin, M. Chhowalla, Z. Zheng, Production of two-dimensional nanomaterials via liquid-based direct exfoliation, Small 12 (2016) 272–293.

[45] R.Y. Tay, H. Li, S.H. Tsang, M. Zhu, M. Loeblein, L. Jing, F.N. Leong, E.H.T. Teo, Trimethylamine borane: a new single-source precursor for monolayer h-BN single crystals and h-BCN thin films, Chem. Mater. 28 (2016) 2180–2190.

[46] M.A. Mannan, M. Nagano, T. Kida, N. Hirao, Y. Baba, Characterization of BCN films synthesized by radiofrequency plasma enhanced chemical vapor deposition, J. Phys. Chem. Solids 70 (2009) 20–25.

[47] O. Baake, P.S. Hoffmann, M.L. Kosinova, A. Klein, B. Pollakowski, B. Beckhoff, N. I. Fainer, V.A. Trunova, W. Ensinger, Analytical characterization of BC x N y films generated by LPCVD with triethylamine borane, Anal. Bioanal. Chem. 398 (2010) 1077–1084.

[48] M.A. Mannan, H. Noguchi, T. Kida, M. Nagano, N. Hirao, Y. Baba, Chemical bonding states and local structures of the oriented hexagonal BCN films synthesized by microwave plasma CVD, Mater. Sci. Semicond. Process. 11 (2008) 100–105.

[49] T. Sugino, T. Tai, Dielectric constant of boron nitride films synthesized by plasma-assisted chemical vapor deposition, Jpn. J. Appl. Phys. 39 (2000) L1101.

[50] J. Yu, E.G. Wang, J. Ahn, S.F. Yoon, Q. Zhang, J. Cui, M.B. Yu, Turbostratic boron carbonitride films produced by bias-assisted hot filament chemical vapor deposition, J. Appl. Phys. 87 (2000) 4022–4025.

[51] T. Yuki, S. Umeda, T. Sugino, Electrical and optical characteristics of boron carbon nitride films synthesized by plasma-assisted chemical vapor deposition, Diam. Relat. Mater. 13 (2004) 1130–1134.

[52] E. Oks, A. Anders, A. Nikolaev, Y. Yushkov, Sputtering of pure boron using a magnetron without a radio-frequency supply, Rev. Sci. Instrum. 88 (2017) 43506.

[53] D.H. Kim, E. Byon, S. Lee, J.-K. Kim, H. Ruh, Characterization of ternary boron carbon nitride films synthesized by RF magnetron sputtering, Thin Solid Films 447 (2004) 192–196.

[54] J.M. Lackner, Industrially-scaled large-area and high-rate tribological coating by pulsed laser deposition, Surf. Coat. Technol. 200 (2005) 1439–1444.

[55] H. Ling, J.D. Wu, J. Sun, W. Shi, Z.F. Ying, F.M. Li, Electron cyclotron resonance plasma-assisted pulsed laser deposition of boron carbon nitride films, Diam. Relat. Mater. 11 (2002) 1623–1628.

[56] I. Jiménez, R. Torres, I. Caretti, R. Gago, J.M. Albella, A review of monolithic and multilayer coatings within the boron–carbon–nitrogen system by ion-beam-assisted deposition, J. Mater. Res. 27 (2012) 743–764.

[57] F. Zhou, K. Adachi, K. Kato, Influence of deposition parameters on surface roughness and mechanical properties of boron carbon nitride coatings synthesized by ion beam assisted deposition, Thin Solid Films 497 (2006) 210–217.

[58] M. Moradi, Y. Vasseghian, A. Khataee, M. Harati, H. Arfaeinia, Ultrasound-assisted synthesis of FeTiO3/GO nanocomposite for photocatalytic degradation of phenol under visible light irradiation, Sep. Purif. Technol. 261 (2021), 118274.

[59] Z. Taherian, A. Khataee, Y. Orooji, Facile synthesis of yttria-promoted nickel catalysts supported on MgO-MCM-41 for syngas production from greenhouse gases, Renew. Sust. Energ. Rev. 134 (2020), 110130.

[60] A. Khataee, T. Sadeghi Rad, S. Nikzat, A. Hassani, M.H. Aslan, M. Kobya, E. Demirbaş, Fabrication of NiFe layered double hydroxide/reduced graphene oxide (NiFe-LDH/rGO) nanocomposite with enhanced sonophotocatalytic activity for the degradation of moxifloxacin, Chem. Eng. J. 375 (2019), 122102, https://doi.org/10.1016/J.CEJ.2019.122102.

[61] G.V. Shahed, Z. Taherian, A. Khataee, F. Meshkani, Y. Orooji, Samarium-impregnated nickel catalysts over SBA-15 in steam reforming of CH4 process, J. Ind. Eng. Chem. 86 (2020) 73–80.

[62] A. Akhundi, A. Badiei, G.M. Ziarani, A. Habibi-Yangjeh, M.J. Muñoz-Batista, R. Luque, Graphitic carbon nitride-based photocatalysts: toward efficient organic transformation for value-added chemicals production, Mol. Catal. 488 (2020), 110902.

[63] N.R.A.M. Shah, R.M. Yunus, N.N. Rosman, W.Y. Wong, K. Arifin, L.J. Minggu, Current progress on 3D graphene-based photocatalysts: from synthesis to photocatalytic hydrogen production, Int. J. Hydrog. Energy 46 (2021) 9324–9340.

[64] H.M. El-Bery, H.N. Abdelhamid, Photocatalytic hydrogen generation via water splitting using ZIF-67 derived Co3O4@ C/TiO2, J. Environ. Chem. Eng. 9 (2021), 105702.

[65] J. Pan, P. Wang, P. Wang, Q. Yu, J. Wang, C. Song, Y. Zheng, C. Li, The photocatalytic overall water splitting hydrogen production of g-C3N4/CdS hollow core–shell heterojunction via the HER/OER matching of Pt/MnOx, Chem. Eng. J. 405 (2021), 126622.

[66] K. Xu, Q. Zhang, C. Wang, J. Xu, Y. Bu, B. Liang, Y. Liu, L. Wang, 0D boron carbon nitride quantum dots decorated 2D Bi4O5I2 as 0D/2D efficient visible-light-driven photocatalysts for tetracyclines photodegradation, Chemosphere 289 (2022), 133230.

[67] K. Xu, Q. Zhang, W. Xu, X. Kang, L. Wang, Er-doping g-C3N4/boron carbon nitride quantum dots composites under visible light irradiation for tetracycline degradation, Mater. Lett. 311 (2022), 131489.

[68] K. Sivaprakash, M. Induja, P.G. Priya, Facile synthesis of metal free non-toxic boron carbon nitride nanosheets with strong photocatalytic behavior for degradation of industrial dyes, Mater. Res. Bull. 100 (2018) 313–321.

[69] J. Shi, T. Yuan, M. Zheng, X. Wang, Metal-free heterogeneous semiconductor for visible-light photocatalytic decarboxylation of carboxylic acids, ACS Catal. 11 (2021) 3040–3047.

[70] S. Wang, W. Zhang, F. Jia, H. Fu, T. Liu, X. Zhang, B. Liu, A. Núñez-Delgado, N. Han, Novel Ag3PO4/boron-carbon-nitrogen photocatalyst for highly efficient degradation of organic pollutants under visible-light irradiation, J. Environ. Manag. 292 (2021), 112763.

[71] S. Ebadi, K. Ghasemipanah, E. Alaie, A. Rashidi, A. Khataee, COD removal from gasfield produced water using photoelectrocatalysis process on coil type microreactor, J. Ind. Eng. Chem. 98 (2021) 262–269.

[72] J. Shi, T. Yuan, R. Wang, M. Zheng, X. Wang, Boron carbonitride photocatalysts for direct decarboxylation: the construction of C (sp 3)–N or C (sp 3)–C (sp 2) bonds with visible light, Green Chem. 23 (2021) 3945–3949.

[73] Z. Hasan, S.H. Jhung, Removal of hazardous organics from water using metal-organic frameworks (MOFs): plausible mechanisms for selective adsorptions, J. Hazard. Mater. 283 (2015) 329–339.

[74] A. Banaei, S. Ebrahimi, H. Vojoudi, S. Karimi, A. Badiei, E. Pourbasheer, Adsorption equilibrium and thermodynamics of anionic reactive dyes from aqueous solutions by using a new modified silica gel with 2, 2′-(pentane-1, 5-diylbis (oxy)) dibenzaldehyde, Chem. Eng. Res. Des. 123 (2017) 50–62.

[75] A. Yadav, S.S. Dindorkar, S.B. Ramisetti, N. Sinha, Simultaneous adsorption of methylene blue and arsenic on graphene, boron nitride and boron carbon nitride nanosheets: insights from molecular simulations, J. Water Process Eng. 46 (2022), 102653.

[76] A. Yadav, S.S. Dindorkar, S.B. Ramisetti, Adsorption behaviour of boron nitride nanosheets towards the positive, negative and the neutral antibiotics: insights from first principle studies, J. Water Process Eng. 46 (2022), 102555.

[77] J. Luo, C. Wang, J. Liu, Y. Wei, Y. Chao, Y. Zou, L. Mu, Y. Huang, H. Li, W. Zhu, High-performance adsorptive desulfurization by ternary hybrid boron carbon nitride aerogel, AIChE J. e17280 (2021).

[78] P. Wang, P. Wang, Y. Guo, L. Rao, C. Yan, Selective recovery of protonated dyes from dye wastewater by pH-responsive BCN material, Chem. Eng. J. 412 (2021), 128532, https://doi.org/10.1016/j.cej.2021.128532.

[79] Y. Guo, C. Yan, P. Wang, L. Rao, C. Wang, Doping of carbon into boron nitride to get the increased adsorption ability for tetracycline from water by changing the pH of solution, Chem. Eng. J. 387 (2020), 124136, https://doi.org/10.1016/j.cej.2020.124136.

[80] X. Zhao, C. Yao, H. Chen, Y. Fu, C. Xiang, S. He, X. Zhou, H. Zhang, In situ nano Au triggered by a metal boron organic polymer: efficient electrochemical N 2 fixation to NH 3 under ambient conditions, J. Mater. Chem. A 7 (2019) 20945–20951.

[81] H. Huang, L. Xia, X. Shi, A.M. Asiri, X. Sun, Ag nanosheets for efficient electrocatalytic N 2 fixation to NH 3 under ambient conditions, Chem. Commun. 54 (2018) 11427–11430.

[82] S. Li, D. Bao, M. Shi, B. Wulan, J. Yan, Q. Jiang, Amorphizing of au nanoparticles by CeOx–RGO hybrid support towards highly efficient electrocatalyst for N2 reduction under ambient conditions, Adv. Mater. 29 (2017) 1700001.

[83] X. Zhao, Z. Yang, A.V. Kuklin, G.V. Baryshnikov, H. Ågren, W. Wang, X. Zhou, H. Zhang, Potassium ions promote electrochemical nitrogen reduction on nano-au catalysts triggered by bifunctional boron supramolecular assembly, J. Mater. Chem. A 8 (2020) 13086–13094.

[84] X. Zhu, T. Wu, L. Ji, C. Li, T. Wang, S. Wen, S. Gao, X. Shi, Y. Luo, Q. Peng, Ambient electrohydrogenation of N 2 for NH 3 synthesis on non-metal boron phosphide nanoparticles: the critical role of P in boosting the catalytic activity, J. Mater. Chem. A 7 (2019) 16117–16121.

[85] L. Xia, J. Yang, H. Wang, R. Zhao, H. Chen, W. Fang, A.M. Asiri, F. Xie, G. Cui, X. Sun, Sulfur-doped graphene for efficient electrocatalytic N 2-to-NH 3 fixation, Chem. Commun. 55 (2019) 3371–3374.

[86] Y. Wang, K. Jia, Q. Pan, Y. Xu, Q. Liu, G. Cui, X. Guo, X. Sun, Boron-doped TiO2 for efficient electrocatalytic N2 fixation to NH3 at ambient conditions, ACS Sustain. Chem. Eng. 7 (2018) 117–122.

[87] C. Chen, D. Yan, Y. Wang, Y. Zhou, Y. Zou, Y. Li, S. Wang, B-N pairs enriched defective carbon nanosheets for ammonia synthesis with high efficiency, Small 15 (2019), 1805029.

[88] C. Lv, Y. Qian, C. Yan, Y. Ding, Y. Liu, G. Chen, G. Yu, Defect engineering metal-free polymeric carbon nitride electrocatalyst for effective nitrogen fixation under ambient conditions, Angew.Chem. 130 (2018) 10403–10407.

[89] X. Zhao, Z. Yang, A.V. Kuklin, G.V. Baryshnikov, H. Ågren, W. Liu, H. Zhang, X. Zhou, BCN-encapsulated Nano-nickel synergistically promotes ambient electrochemical dinitrogen reduction, ACS Appl. Mater. Interfaces 12 (2020) 31419–31430.

[90] X. Zhao, G. Hu, F. Tan, S. Zhang, X. Wang, X. Hu, A.V. Kuklin, G.V. Baryshnikov, H. Ågren, X. Zhou, Copper confined in vesicle-like BCN cavities promotes electrochemical reduction of nitrate to ammonia in water, J. Mater. Chem. A 9 (2021) 23675–23686.

[91] X. Zhao, Z. Zhu, Y. He, H. Zhang, X. Zhou, W. Hu, M. Li, S. Zhang, Y. Dong, X. Hu, Simultaneous anchoring of Ni nanoparticles and single-atom Ni on BCN matrix promotes efficient conversion of nitrate in water into high-value-added ammonia, Chem. Eng. J. 133190 (2021).

[92] X. Zhao, X. Li, H. Zhang, X. Chen, J. Xu, J. Yang, H. Zhang, G. Hu, Atomic-dispersed copper simultaneously achieve high-efficiency removal and high-value-added conversion to ammonia of nitrate in sewage, J. Hazard. Mater. 424 (2022), 127319.

[93] X. Zhao, X. Jia, Y. He, H. Zhang, X. Zhou, H. Zhang, S. Zhang, Y. Dong, X. Hu, A. V. Kuklin, Two-dimensional BCN matrix inlaid with single-atom-Cu driven electrochemical nitrate reduction reaction to achieve sustainable industrial-grade production of ammonia, Appl. Mater. Today 25 (2021), 101206.
[94] V. Vatanpour, S. Paziresh, S. Ali, N. Mehrabani, S. Feizpoor, A. Habibi-yangjeh, I. Koyuncu, TiO2/CDs modified thin-film nanocomposite polyamide membrane for simultaneous enhancement of antifouling and chlorine-resistance performance, Desalination 525 (2022), 115506, https://doi.org/10.1016/j.desal.2021.115506.
[95] A.Y. Goren, H.E. Okten, Simultaneous energy production, boron and COD removal using a novel microbial desalination cell, Desalination 518 (2021), 115267.
[96] M. Kobya, R.D.C. Soltani, P.I. Omwene, A. Khataee, A review on decontamination of arsenic-contained water by electrocoagulation: reactor configurations and operating cost along with removal mechanisms, Environ. Technol. Innov. 17 (2020), 100519, https://doi.org/10.1016/j.eti.2019.100519.
[97] Z. Ding, X. Xu, J. Li, Y. Li, K. Wang, T. Lu, M.S.A. Hossain, M.A. Amin, S. Zhang, L. Pan, Nanoarchitectonics from 2D to 3D: MXenes-derived nitrogen-doped 3D nanofibrous architecture for extraordinarily-fast capacitive deionization, Chem. Eng. J. 430 (2022), 133161.
[98] L.D. Nguyen, Q. Van Nguyen, N.T.T. Nguyen, T.C.D. Doan, D.M.T. Dang, C. M. Dang, Designing, fabricating and testing at a laboratory scale a water desalination system using electrodialysis, Sci. Technol. Dev. J.-Nat. Sci. 6 (2022) press-press.
[99] M. Ghasemi, A. Khataee, P. Gholami, R.D.C. Soltani, A. Hassani, Y. Orooji, In-situ electro-generation and activation of hydrogen peroxide using a CuFeNLDH-CNTs modified graphite cathode for degradation of cefazolin, J. Environ. Manag. 267 (2020), 110629, https://doi.org/10.1016/J.JENVMAN.2020.110629.
[100] J. Li, B. Ji, R. Jiang, P. Zhang, N. Chen, G. Zhang, L. Qu, Hierarchical hole-enhanced 3D graphene assembly for highly efficient capacitive deionization, Carbon N. Y. 129 (2018) 95–103.
[101] O. Sufiani, H. Tanaka, K. Teshima, R.L. Machunda, Y.A.C. Jande, Enhanced electrosorption capacity of activated carbon electrodes for deionized water production through capacitive deionization, Sep. Purif. Technol. 247 (2020), 116998.
[102] P. Liu, T. Yan, J. Zhang, L. Shi, D. Zhang, Separation and recovery of heavy metal ions and salt ions from wastewater by 3D graphene-based asymmetric electrodes via capacitive deionization, J. Mater. Chem. A 5 (2017) 14748–14757.
[103] X. Gao, A. Omosebi, J. Landon, K. Liu, Enhanced salt removal in an inverted capacitive deionization cell using amine modified microporous carbon cathodes, Environ. Sci. Technol. 49 (2015) 10920–10926.
[104] N. Lee, M.-L. Liu, M.-C. Wu, T.-H. Chen, C.-H. Hou, The effect of redox potential on the removal characteristic of divalent cations during activated carbon-based capacitive deionization, Chemosphere 274 (2021), 129762.
[105] G. Bharath, A. Hai, K. Rambabu, T. Pazhanivel, S.W. Hasan, F. Banat, Designed assembly of Ni/MAX (Ti3AlC2) and porous graphene-based asymmetric electrodes for capacitive deionization of multivalent ions, Chemosphere 266 (2021), 129048.
[106] W. Zhang, X. Wei, X. Zhang, S. Huo, A. Gong, X. Mo, K. Li, Well-dispersed prussian blue analogues connected with carbon nanotubes for efficient capacitive deionization process, Sep. Purif. Technol. 120483 (2022).
[107] H.H. Kyaw, M.T.Z. Myint, S. Al-Harthi, H. Ala'a, M. Al-Abri, Electric field enhanced in situ silica nanoparticles grafted activated carbon cloth electrodes for capacitive deionization, Sep. Purif. Technol. 281 (2022), 119888.
[108] S. Kumar, G. Saeed, L. Zhu, K.N. Hui, N.H. Kim, J.H. Lee, 0D to 3D carbon-based networks combined with pseudocapacitive electrode material for high energy density supercapacitor: a review, Chem. Eng. J. 403 (2021), 126352.
[109] B. Samejo, S. Gul, S. Samejo, N.Q. Abro, N. Yenil, N. Memon, Carbon based electrode materials and their architectures for capacitive deionization, Pak. J. AnalEnviron. Chem. 22 (2021) 210–242.
[110] P. Gholami, A. Khataee, R.D.C. Soltani, A. Bhatnagar, A review on carbon-based materials for heterogeneous sonocatalysis: fundamentals, properties and applications, Ultrason. Sonochem. 58 (2019), 104681.
[111] K. Qi, N. Cui, M. Zhang, Y. Ma, G. Wang, Z. Zhao, A. Khataee, Ionic liquid-assisted synthesis of porous boron-doped graphitic carbon nitride for photocatalytic hydrogen production, Chemosphere 272 (2021), 129953.
[112] J. Azamat, A. Khataee, F. Sadikoglu, Separation of carbon dioxide and nitrogen gases through modified boron nitride nanosheets as a membrane: insights from molecular dynamics simulations, RSC Adv. 6 (2016) 94911–94920.
[113] R. Jalili, S. Chenaghlou, A. Khataee, B. Khalilzadeh, M.-R. Rashidi, An electrochemiluminescence biosensor for the detection of Alzheimer's tau protein based on gold nanostar decorated carbon nitride nanosheets, Molecules 27 (2022) 431.
[114] H. Sohrabi, O. Arbabzadeh, P. Khaaki, A. Khataee, M.R. Majidi, Y. Orooji, Patulin and trichothecene: characteristics, occurrence, toxic effects and detection capabilities via clinical, analytical and nanostructured electrochemical sensing/biosensing assays in foodstuffs, Crit. Rev. Food Sci. Nutr. 1–29 (2021).
[115] R. Jalili, A. Khataee, M.-R. Rashidi, A. Razmjou, Detection of penicillin G residues in milk based on dual-emission carbon dots and molecularly imprinted polymers, Food Chem. 314 (2020), 126172.
[116] Y. Orooji, M. Haddad Irani-nezhad, R. Hassandoost, A. Khataee, S. Rahim Pouran, S.W. Joo, Cerium doped magnetite nanoparticles for highly sensitive detection of metronidazole via chemiluminescence assay, Spectrochim. Acta Part A Mol. Biomol. Spectrosc. 234 (2020), 118272, https://doi.org/10.1016/J.SAA.2020.118272.
[117] S. Wang, G. Wang, T. Wu, Y. Zhang, F. Zhan, Y. Wang, J. Wang, Y. Fu, J. Qiu, BCN nanosheets templated by gC 3 N 4 for high performance capacitive deionization, J. Mater. Chem. A 6 (2018) 14644–14650.